https://www.science.org/doi/full/10.1126/scisignal.aba5754

One-sentence summary: Binge drinking may cause anxiety by triggering microglia to destroy excitatory synapses.

Daily alcohol intake triggers aberrant synaptic pruning leading to synapse loss and anxiety-like behavior

Renato Socodato[1,*,#], Joana F. Henriques[*,1], Camila C. Portugal[*,1], Tiago O. Almeida[1], Joana Tedim-Moreira[1], Renata L. Alves[1], Teresa Canedo[1, 2], Cátia Silva[1], Ana Magalhães[1], Teresa Summavielle[1,#] and João B. Relvas[1,2,#]

[1]Instituto de Investigação e Inovação em Saúde and Instituto de Biologia Molecular e Celular, Universidade do Porto, 4200-135 Porto, Portugal.

[2] Department of Biomedicine, Faculty of Medicine, University of Porto, 4200-319 Porto, Portugal.

*These authors contributed equally.

[#]Corresponding authors. Emails: renato.socodato@ibmc.up.pt (R.S.), tsummavi@ibmc.up.pt (T.S.), and jrelvas@ibmc.up.pt (J.B.R.).

Abstract

Alcohol abuse adversely impacts the lives of millions of people worldwide. Deficits in synaptic transmission and in microglial function are commonly found in human alcohol abusers and in animal models of alcohol intoxication. Here, we found that a protocol simulating chronic binge drinking in male mice resulted in aberrant synaptic pruning and substantial loss of excitatory synapses in the prefrontal cortex, which resulted in increased anxiety-like behavior. Mechanistically, alcohol intake increased the engulfment capacity of microglia in a manner dependent on the kinase Src, the subsequent activation of the transcription factor NF-kB, and the consequent production of the proinflammatory cytokine TNF. Pharmacological blockade of Src activation or of TNF production in microglia, genetic ablation of *Tnf*, or conditional ablation of microglia attenuated aberrant synaptic pruning, thereby preventing the neuronal and behavioral effects of the alcohol. Our data suggest that aberrant pruning of excitatory synapses by microglia may disrupt synaptic transmission in response to alcohol abuse.

Introduction

Alcohol abuse is associated with pathophysiological changes in the brain and peripheral organs, many of which can result in life-threatening conditions. The effects of alcohol in the central nervous system (CNS) often lead to behavioral deficits (including anxiety, cognitive decline, and motor dysfunction) and impairment of synaptic function, a major hallmark of alcohol abuse, likely underlies such behavioral deficits. Indeed, alcohol detrimentally impacts the pre- and postsynaptic compartments and the secretion/recycling of neurotransmitters, ultimately leading to the disruption of excitatory and inhibitory neurotransmission (*1, 2*). This detrimental effect of alcohol on synapses can be contributed by a well-established action of alcohol on neurons and, potentially, through an underappreciated action of alcohol on glial cells (*3*).

Microglia, the major innate immune cell population in the brain (*4*), maintain nervous tissue homeostasis, surveilling the CNS parenchyma by continuously extending and retracting their cellular processes, monitoring for tissue damage or infections and checking the functional status of synapses (*5*). Upon CNS tissue damage or infection, microglia become activated, changing their morphology (into a more ameboid shape), phagocytic capacity, and transcriptional profile to restore tissue homeostasis (*5*). In many neuropsychiatric disorders, however, microglia immune function becomes impaired, often leading to overproduction of inflammatory mediators and exacerbated phagocytic activity, which can be detrimental to synapses and negatively affect behavior (*6, 7*).

In human alcohol abusers (*8*) and in animal models of alcohol intoxication (*9*), alteration of microglial function associates with neuroimmune activation (*10, 11*) and may be directly involved in some of the neurotoxic and adverse behavioral effects of alcohol intake (*12*). Indeed, activation of the innate immune system contributes to neuroadaptations in brain regions linked with escalating alcohol consumption, tolerance, dependence, and relapse (*13, 14*). Consistent with a neuroimmune hypothesis for alcohol addiction (*11*), knocking out various genes involved in immune

responses, which in the brain are exclusively expressed or highly enriched in microglia, decreases voluntary alcohol intake in mice.

In this study, we found that binge-level alcohol intake (about 5 drinks for an average person) over ten consecutive days enhanced Src-to-TNF signaling in prefrontal cortex microglia, which boosted their engulfment capacity and led to aberrant synaptic pruning, culminating in synapse loss and anxiety-like behavior. Overall, our data suggest that aberrant synaptic pruning by microglia might play an important role in the synaptic transmission deficits elicited by alcohol abuse.

Results

Alcohol intake produces a microglia-driven neuroimmune response in the prefrontal cortex

In mouse models of alcohol intoxication, alcohol intake leads to microglia activation and oxidative damage (*15*). We sought to study the effect of alcohol intake on microglia reactivity and used a protocol of ethanol (EtOH) exposure simulating repetitive binge-level drinking. For this, we administrated 1.5 g/Kg of EtOH (a dosage equivalent to 5 drinks for an adult person weighing 75 kg) or water (H_2O) for ten consecutive days to a microglia reporter [$Cx3cr1^{EYFP\text{-}CreER/+}$ (*16*)] mouse (**Fig. 1A**). Immunohistochemistry on prefrontal cortex tissue sections from $Cx3cr1^{EYFP\text{-}CreER/+}$ mice revealed that this EtOH exposure protocol induced a significant expansion of prefrontal cortex microglia (YFP^+ cells, **Fig. 1B**). Using flow cytometry, we confirmed this increased number of microglia in $Cx3cr1^{EYFP\text{-}CreER/+}$ mice gavaged with EtOH (**Fig. 1C**). EtOH also increased the expression of the reactivity markers CD45, integrin alpha M (CD11b), and Iba1 in prefrontal cortex microglia (**Fig. 1, C and D**). Morphometry of prefrontal cortex microglia (identified by Iba1 labeling) using Sholl analysis revealed that EtOH induced microglia hyperamification, meaning increased branching (or intersections) and process number without affecting process length (**Fig. 1E**). EtOH

significantly altered the expression levels of the microglia-enriched mRNA transcripts *P2ry12*, *Pu.1*, *Gpr34*, *Csfr1*, *C1qC*, *Tgfβr1*, *C1qB*, *Mertk*, *Tlr4*, *Trem2* and *C1qA* in the neocortex of Cx3cr1$^{EYFP\text{-}CreER/+}$ mice (**Fig. 1F**). Enrichment analysis based on gene ontology using those altered transcripts revealed that several immune-associated pathways were significantly modified by EtOH intake, including pathways altering microglial activity, innate immune response, and TNF–NF-kB signaling (**Fig. 1G**).

The effect of EtOH on microglia was also confirmed in wild-type mice, displaying similar results regarding microglial cell number (**fig. S1A**), microglia-enriched mRNA transcripts (**fig. S1B**) and microglia morphology (**fig. S1C**) compared with Cx3cr1$^{EYFP\text{-}CreER/+}$ mice that carry only one functional *Cx3cr1* allele. We then evaluated the effect of alcohol on other immune cell populations. Compared with water-treated controls, EtOH did not alter the number of macrophages (EYFP^{+}CD11b^{+}CD45^{hi} cells), B lymphocytes (CD19^{+}CD45^{+}CD11b^{-}EYFP^{-} cells) or T lymphocytes (CD3^{+}CD45^{+}CD11b^{-}EYFP^{-} cells) in the neocortex of Cx3cr1$^{EYFP\text{-}CreER/+}$ mice (**fig. S1, D to F**). Astrocytes also perform immune cell functions within the brain parenchyma, and alcohol exposure leads to astrocytic activation through several mechanisms (*15, 17-22*). Therefore, we tested whether our EtOH exposure protocol would modulate astrocytic reactivity. We found no significant difference in the number of prefrontal cortex astrocytes (GFAP^{+} cells) or in the expression of GFAP in EtOH-treated mice (**fig. S1, G and H**), which might suggest that our experimental paradigm of repetitive binge-level drinking did not produce a strong reaction in astrocytes.

Because our alcohol exposure protocol triggered microgliosis, we evaluated the transcript abundance of genes involved in classical immune responses and antioxidant defenses in mice exposed to EtOH. We found that EtOH increased the transcript levels of *Tlr2*, *Cd14*, *Icam1*, *Slc23a2*, *Tspo*, *Tnf*, *Rip1*, *Traf2* and decreased the transcript levels of *Il-6*, *Ccl5*, *Tlr7*, *Mhc-II*, *Gclc*, *Traf1*, *Ccl2*, *Hmox1*, *Cox2*, *Irak3*, *Tnxnrd1* and *Gsr* in the neocortex of Cx3cr1$^{EYFP\text{-}CreER/+}$ mice (**Fig. 2A**). Moreover, other immune-related genes such as *Il-18*, *Il-1b*, *Inf-b*, *Cd163*, *Socs3*, *Nrlp3*, *Nos2*, *Cx3cl1*,

Cxcl10, *Arg1*, *Mrp8*, *Mrp14*, *Cxcl1,* and *Spp1* were not significantly altered by EtOH (**Fig. 2B**). Pathway analysis of the differentially expressed genes following EtOH exposure revealed a substantial number of significantly enriched pathways that were both directly and indirectly modulated by TNF (**Fig. 2C**). The majority of those enriched pathways were related to immune responses but also included cell migration, cell proliferation, cell adhesion, intracellular signal transduction, and cytokine biosynthesis and secretion (**Fig. 2C**). Network analysis of protein-protein interactions revealed the prevalence of ten major protein clusters to be modulated by EtOH intake (**Fig. 2D**). The TNF cluster was more intricately associated with TLR2 and IRAK3 clusters (**Fig. 2D**), suggesting that the alteration of neuroimmune pathways following EtOH exposure might be co-regulated via TNF, TLR2, and IRAK3. In addition, several interacting proteins within the TNF cluster (**Fig. 2D**), are known modulators/integrators of brain immune responses and microglial activation, thereby indicating that the neuroimmune response triggered by EtOH intake might be strongly associated with TNF.

Preventing TNF production suppresses microglia activation after alcohol intake

Microglia are critical producers of TNF after acute binge alcohol intake (*23*). To test whether microglia were also major producers of TNF during our alcohol exposure protocol, we genetically ablated microglia using a microglial iDTR/Cre-lox system (*16*). We first validated the efficiency of this microglia ablation system in the context of our experimental requirements by giving tamoxifen to Cx3cr1$^{EYFP\text{-}CreER/+}$:R26$^{iDTR/+}$ and Cx3cr1$^{EYFP\text{-}CreER/+}$ mice at P28 and P30 and diphtheria toxin (DT) 2 months later (**Fig. 3A**). Indeed, both immunohistochemistry on prefrontal cortex tissue sections and flow cytometry showed, as expected, that microglia were efficiently eliminated in Cx3cr1$^{EYFP\text{-}CreER/+}$:R26$^{iDTR/+}$ mice (**Fig. 3, B and C**).

Next, we evaluated the production of TNF in the prefrontal cortex of Cx3cr1$^{EYFP\text{-}CreER/+}$ and microglia-depleted (Cx3cr1$^{EYFP\text{-}CreER/+}$:R26$^{iDTR/+}$) mice following EtOH exposure (**Fig. 3D**). Whereas EtOH significantly increased the mRNA and the protein

amounts of TNF in Cx3cr1$^{EYFP\text{-}CreER/+}$ mice (**Fig. 3, E and F**), it did not increase the amounts of TNF in microglia-depleted mice (**Fig. 3, E and F**), suggesting that microglia are the primary producers of TNF in the prefrontal cortex during EtOH exposure.

We next used TNF-deficient (TNF KO) mice or the immunomodulatory and brain-penetrant TNF blocker pomalidomide (PMD) (*24-26*) to test whether TNF production could lead to microgliosis. Using flow cytometry, we found that the EtOH-induced microgliosis (**Fig. 3G**) was prevented entirely in TNF KO mice (**Fig. 3G**) or wild-type mice treated with PMD (**Fig. 3G**). The EtOH-induced alteration of the microglia enriched genes *P2ry12*, *Pu.1*, *Gpr34*, *Csfr1*, *C1qC*, *Tgfβr1*, *Mertk*, *Tlr4*, *Trem2,* and *C1qA* was also abrogated in TNF KO mice (**Fig. 3H**), indicating that microglial TNF is involved in the microgliosis elicited by EtOH exposure.

Alcohol intake modulates the Src–NF-κB pathway to increase TNF production and trigger microglia activation

Because the tyrosine kinase Src controls microglial activation via increased production and secretion of TNF (*27-29*), we investigated whether EtOH could trigger the production of TNF in microglia via Src. We found that the amount of active Src (phospho-Src Tyr^{146}) was significantly increased in the prefrontal cortex of Cx3cr1$^{EYFP\text{-}CreER/+}$ mice exposed to EtOH (**Fig. 4A**) but not in the prefrontal cortex of microglia-depleted mice exposed to EtOH (**Fig. 4A)**. In line with this, the effect of alcohol in increasing microglial Src activation was thoroughly reproduced in a cell autonomous manner in primary cortical microglia [analyzed by immunocytochemistry with an antibody against phospho-Src Tyr^{146} (**fig. S2A**)] and in the CHME3 microglial cell line [analyzed by live-cell imaging using a FRET-based Src biosensor (**fig. S2B**)].

To confirm the relationship between Src activity and TNF expression, we used the clinically relevant Src blocker AZD0530 (*30, 31*) during EtOH exposure. We found that inhibiting Src with AZD0530 (**fig. S2C**) abrogated the increase in TNF elicited by EtOH (**Fig. 4B**). To further confirm that alcohol modulates microglial Src to increase

the production of TNF, we inhibited Src, using the Src blocker SKI-1, in primary cortical microglia and found that SKI-1 prevented the alcohol-mediated increase of TNF production (**fig. S2D**).

To gain further mechanistic insight into how Src drives TNF production in microglia during alcohol exposure, we focused on the role of NF-kB, a central regulator of inflammatory signaling in immune cells (*32, 33*). We measured the nuclear accumulation of the p65 subunit of NF-kB as a functional indicator of NF-kB activation in CHME3 microglia using a green fluorescent protein (GFP)–tagged p65 construct. We found that exposure to alcohol increased nuclear GFP content in CHME3 microglia (**Fig. 4C**), and that knocking down Src (**fig. S2E**) abrogated the alcohol-induced nuclear translocation of GFP-p65 subunit (**Fig. 4C**). Pharmacological blockade of Src using AZD0530 or SKI-1 also prevented the alcohol-induced activation of the NF-κB pathway, monitored using the IκBα-miRFP703 reporter (*34*) (**fig. S2F**) Moreover, direct activation of Src in CHME3 microglia, using rapamycin-based chemogenetics with RapR-Src/FRB (*35*), increased the nuclear translocation of the GFP-p65 subunit (**fig. S2G**). Paralleling the increase of NF-kB activation following Src activation, overexpressing the constitutively active Src mutant Src^{Y527F} led to increased secretion of TNF from microglia (**fig. S2H**). Finally, preventing NF-kB activation with the clinically relevant inhibitor sulfasalazine (*36, 37*) completely blocked the production of TNF elicited by Src^{Y527F} in microglia (**Fig. 4D**). These data suggest that alcohol drives TNF production in microglia via Src and downstream NF-kB activation.

In line with such Src-dependent TNF production during alcohol exposure, in vivo blockade of Src with AZD0530 abrogated the EtOH-induced increase of microglial numbers and prevented the EtOH-mediated alteration of the microglia-enriched genes *P2ry12*, *Pu.1*, *Gpr34*, *Csfr1*, *C1qC*, *Tgfβr1*, *Mertk*, *Tlr4*, *Trem2* and *C1qA* (**Fig. 4, E and F**).

Blocking microglial TNF signaling suppresses anxiety-like behavior elicited by alcohol intake

The neuroimmune hypothesis of alcohol addiction (*11*) supports the notion that alterations of neuroimmune signaling might be responsible for some of the behavioral deficits elicited by alcohol abuse. Because EtOH induced the production of TNF by prefrontal cortex microglia, we tested whether EtOH could drive changes in behavior. We found, using the elevated-plus maze (EPM) test, that EtOH increased anxiety-like behavior in adult Cx3cr1$^{EYFP\text{-}CreER/+}$ mice, as revealed by the decreased time that EtOH-subjected mice spent on the open arms (**Fig. 5A**). No differences were found in the distance traveled in the EPM between EtOH-treated and water-treated mice (**Fig. 5B**). The anxiogenic effect of EtOH could also be observed in wild-type mice in the EPM test (**fig. S3, A and B**). Moreover, the increase of anxiety-like behavior elicited by EtOH exposure was reproduced in the open field test, as mice exposed to EtOH spent less time in the center of the open field arena than water-treated littermates (**fig. S3C**).

EtOH did not produce significant changes in (1) general locomotor activity (**fig. S3D**) or repetitive behavior (**fig. S3E**) when mice were evaluated in the open field test, and in (2) recognition memory when mice were assessed on the novel object recognition test (**fig. S3, F and G**).

We then investigated whether the anxiogenic effect of EtOH intake required the production of TNF by microglia. We found that blocking TNF production indirectly (by inhibiting Src with AZD0530) or directly (by inhibiting TNF expression with PMD) completely suppressed the EtOH-induced increase in anxiety-like behavior (**Fig. 5, A and B**). To further confirm the role of microglia in the anxiogenic effect of EtOH intake, we evaluated microglia-depleted mice in the EPM test. Whereas EtOH increased anxiety-like behavior in control (Cx3cr1$^{EYFP\text{-}CreER/+}$) mice, this effect was significantly prevented in microglia-depleted (Cx3cr1$^{EYFP\text{-}CreER/+}$:R26$^{iDTR/+}$) mice (**Fig. 5C**). No differences were found in the distance traveled in the EPM between the genotypes or treatment groups (**Fig. 5D**).

Alcohol-induced TNF signaling increases microglia phagocytic activity, enabling microglia to prune prefrontal cortex synapses

Behavioral alterations, such as increased anxiety, can be caused by perturbations in the excitatory/inhibitory balance in prefrontal cortex circuits (*38, 39*) and exacerbation of microglia activation decreases the number of excitatory synapses in the neocortex (*40*). Indeed, we found that the amounts of PSD-95 and vGlut1 (major proteins involved in excitatory synaptic transmission) along with the number of excitatory synapses ($PSD\text{-}95^+/vGlut1^+$ puncta) were significantly decreased in prefrontal cortices of mice exposed to EtOH (**Fig. 6A and fig. S4A**). The decrease of PSD-95 puncta, vGlut1 puncta, and $PSD\text{-}95^+/vGlut1^+$ synapses elicited by EtOH intake were prevented in TNF KO mice (**Fig. 6A and fig. S4A**) and in microglia-depleted mice (**Fig. 6B and fig. S4B**). Biochemical assessment further confirmed that EtOH intake decreased, in a microglia-dependent manner, the amounts of PSD-95 and vGlut1 in the prefrontal cortex (**Fig. 6C**), indicating that TNF production by microglia leads to loss of excitatory synapses in the prefrontal cortex following EtOH intake.

Loss of synapses can be a consequence of increased neuronal cell death. However, we found that the number of neurons (stained with NeuN) in the prefrontal cortex was not significantly different between EtOH-subjected and water-treated mice (**fig. S4C**). The numbers of excitatory synapses in the CA1 region of the dorsal hippocampus of EtOH-subjected mice were not significantly different from those of water-treated littermates (**fig. S5A**), which may help to explain the specificity of the behavioral phenotype elicited by EtOH.

In pathological conditions, such as in Alzheimer's disease, microglia can phagocytose and prune healthy synapses; a process termed synaptophagy (*7*). We hypothesized that the EtOH-mediated loss of excitatory synapses in the prefrontal cortex could be a direct consequence of excessive engulfment of synaptic structures by microglia. To investigate whether microglia exposed to EtOH engulfed more

synapses in vivo, we evaluated by immunofluorescence on prefrontal cortex tissue sections the amount of PSD-95$^+$ puncta within phagocytic structures (labeled with CD68) in Iba1$^+$ microglia. Confocal imaging coupled with 3D cell surface rendering revealed that Iba1$^+$ microglia from the prefrontal cortex of mice exposed to EtOH contained significantly more PSD-95$^+$ puncta colocalizing with CD68 structures than prefrontal cortex microglia from mice gavaged with water (**Fig. 7A**). This microglial engulfment of prefrontal cortex postsynaptic elements required TNF signaling because no significant differences in the engulfment of PSD-95$^+$ puncta were observed in TNF KO mice exposed to EtOH (**Fig. 7A**). Conversely, EtOH neither increased PSD-95 engulfment by Iba1$^+$ microglia in the CA1 region of the dorsal hippocampus (**fig. S5B**) nor triggered the production of TNF in the dorsal hippocampus (**fig. S5C**).

To further assess the engulfment of synapses by microglia, we prepared synaptosomes (to isolate synaptic terminals) from the prefrontal cortex of adult mice and incubated microglial cultures with them. Indeed, immunofluorescence labeling of PSD-95 confirmed that microglia efficiently engulfed synaptosomes prepared from the prefrontal cortex (**Fig. 7B**), further confirming that microglia actively phagocytose synapses in steady-state conditions. However, cultured microglia exposed to EtOH engulfed significantly more prefrontal cortex synaptosomes than control microglia (**Fig. 7B**). To further corroborate the excessive EtOH-mediated engulfment of synaptic structures, microglia cultures were incubated with synaptosomes prepared from the prefrontal cortex of Thy1-YFP mice. Measuring microglia engulfment capacity by flow cytometry revealed that microglia exposed to EtOH displayed significantly increased engulfment of YFP$^+$ synaptosomes compared with control microglia (**Fig. 7C**). Blocking TNF with the neutralizing antibody adalimumab (HUMIRA) completely prevented the engulfment of YFP$^+$ synaptosomes elicited by exposure to EtOH (**Fig. 7C**).

In line with the view that EtOH intake increases microglia engulfment capacity, mice exposed to EtOH displayed a TNF-dependent increase of the microglia engulfment module (represented by transcripts coding for *Adam12*, *Apoe*, *Axl*, *Ccr1*,

CD93, *Cybb*, *Lyz2*, *Mrc1,* and *Siglec1*) (*41*) (**Fig. 7D**) and had a TNF-dependent increase of prefrontal cortex microglia expressing the phagocytic marker CD68 (**Fig. 7E**). In this context, TNF signaling enabled microglial phagocytosis because EtOH increased the phagocytic activity of cortical microglia from wild-type mice but not of cortical microglia from TNF KO mice (**Fig. 7F**). These data suggest that EtOH intake results in aberrant pruning of prefrontal cortex excitatory synapses through microglial TNF signaling.

Discussion

Neuroinflammation is regarded as a major contributing factor in alcohol-induced brain damage (*42-45*). Various studies (including chronic 20 weeks drinking—around 140 mg/dL—in 7 week-old female mice (*46*), and chronic five weeks liquid diet feeding—around 215 mg/dL—in 6 to 8 week-old female mice (*47, 48*)) show that heavy alcohol intake triggers a proinflammatory signature with concomitant gliosis. However, despite inducing neuroimmune activation and excitatory synapse loss, our model of repetitive binge-level alcohol intake in male mice did not produce a classical proinflammatory signature. Rather, our data are more in line with several transcriptomic studies (*49-53*) and specifically one RNA-sequencing study wherein microglia from the prefrontal cortex of mice chronically exposed to alcohol (using the every-other-day, two-bottle choice paradigm) do not induce a classic proinflammatory signature (*54*). Likewise, transcript expression of TLR4 was rather decreased in our EtOH exposure model, which is more in line with studies showing that acute alcohol exposure to human peripheral blood monocytes in culture suppresses TLR4 signaling (*55-58*). Thus, the dose and duration of EtOH exposure appear to differentially affect neuroimmune activation and microglia proinflammatory signaling.

In our study, gene ontology with pathway enrichment indicated that TLR2 and the proinflammatory cytokine TNF were induced upon EtOH intake and that these pathways may be co-regulated in microglia. TLR2-dependent recruitment and activation of the kinase Src stimulate several immune-related pathways, including NF-

κB activation (*59*), phospholipase C-to-integrin engagement (*60*), reactive oxygen species generation (*61*) interleukin-12 production (*62*) and, ultimately, production of proinflammatory mediators—including TNF—by microglia (*29, 30*). EtOH increased Src activation, leading to the nuclear translocation of the p65 subunit of the NF-κB complex, which culminated in NF-κB-dependent TNF production and secretion from microglia. Paralleling the effect of the blockade of TNF production with pomalidomide, inhibiting Src with AZD0530 (a clinically relevant Src inhibitor) also prevented microgliosis. The Src inhibitor also suppressed anxiety-like behavior elicited by EtOH intake, suggesting that targeting the Src–NF-κB–TNF pathway in microglia may prevent the anxiogenic effect of alcohol. The precise signaling mechanism(s) by which alcohol exposure elicits microglial Src activation and NF-κB-dependent transcription warrants further investigation. Likewise, although our microglial ablation experiments demonstrated that microglia were major producers of TNF in the prefrontal cortex during EtOH exposure, we cannot rule out that TNF produced in the periphery (the liver for instance) or even by astrocytes in response to EtOH may also have contributed to the observed microglial phenotype.

The prefrontal cortex contains glutamatergic excitatory neurons that synapse locally or project distally to cortical and subcortical nuclei. Failure to set up and sustain proper excitatory connectivity leads to imbalanced neuronal activity across networks (*63*), which could explain at least some of the behavioral impairments found in various neurological disorders (*26*). Accordingly, the loss of prefrontal cortex excitatory synapses elicited by EtOH could be sufficient to disrupt the excitatory/inhibitory balance of prefrontal cortex neurons that project to anxiety-related centers in subcortical regions, implying that EtOH-induced prefrontal cortex synapse loss might directly impact alcohol-related anxiety. Although this is plausible, our data do not formally exclude the possibility that microglia could be directly activated in other brain regions (such as the amygdala) to elicit the anxiogenic effect of EtOH. Anxiety has also been associated with alcohol withdrawal; however, because our behavior analyses

were carried out at a time-point at which the mice may be expected to have a blood EtOH level of 100-120 mg/dl (*64, 65*), the increased anxiety-like behavior we observed likely reflects a more persistent anxious state driven by consecutive EtOH intake rather than withdrawal-induced anxiety.

A caveat of this study is that the observed phenotypes were only reported for male mice. Sex differences in the emotional responses of mice, such as those related to anxiety-like behavior, are well documented and likely relate to variations in the amounts of sex hormones during the estrous cycle (*66*). The transcriptional program of female and male microglia also vary substantially (*67*), which, together with the fact that female mice are more prone to develop alcohol-related inflammation and neuronal damage (*68, 69*), indicate that further studies using female mice are required to understand better the contribution of EtOH exposure to microglia-dependent synaptic pruning, synapse function and anxiety-related behavior.

Microglia participate in synaptic remodeling by phagocytic engulfment of synaptic terminals (*70*). We found that EtOH exposure increased the engulfment of synaptic structures by microglia likely through enhancing their phagocytic capacity. In contrast, EtOH decreases microglia phagocytosis of *E. coli* (*71*) and amyloid (*72*) and also suppresses microglia phagocytosis stimulated by activation of P2X4 receptors (*73*), thereby suggesting that EtOH might alter microglia phagocytic capacity in a context-specific manner. In addition, given that clearance activity by microglia varies substantially across different brain regions (*41*), it is conceivable that prefrontal cortex microglia were more prone to engulf and prune synapses than their hippocampal counterparts upon exposure to alcohol. While further in-depth studies to identify the precise mechanisms underlying such regional differences and microglial heterogeneity are warranted, our findings that microglia can engulf postsynaptic elements in the prefrontal cortex provides important new mechanistic evidence into how the brain immune system may contribute to impaired synaptic transmission, a major detrimental consequence of alcohol abuse.

Materials and Methods

Animals: All mice experiments were reviewed by i3S animal ethical committee and were approved by Direção-Geral de Alimentação e Veterinária (DGAV). Animals were maintained in standard laboratory conditions with an inverted 12h/12h light-dark cycle and were allowed free access to food and water. Mice were housed under specific pathogen-free conditions. Experiments were carried out following the 3Rs ethics policy, and mice were kept on a C57BL/6 background. Because of the potential behavioral variability related to the estrous cycle in females (*66*), as well as to minimize intergroup variability and limit the number of animals, only male mice (16-20 week-old) were used in this study.

B6.129P2(Cg)-*Cx3cr1*$^{tm2.1(cre/ERT2)Litt}$/WganJ mice (herein referred to as Cx3cr1$^{EYFP\text{-}CreER/+}$; The Jackson Laboratory Stock No: 021160; RRID:IMSR_JAX:021160) mice were used to study brain microglia in this work and were maintained as before (*40*). These mice express a Cre-ERT2 fusion protein and an enhanced yellow fluorescent protein (EYFP) from the endogenous Cx3cr1 promoter. EYFP fluorescence is observed in more than 95% of Iba1^{+} microglia in the brain (*16, 40*).

For microglial cell ablation experiments, Cx3cr1$^{EYFP\text{-}CreER/+}$ mice were intercrossed with R26$^{iDTR/+}$ (*C57BL/6-Gt(ROSA)26Sor*$^{tm1(HBEGF)Awai}$*/J*; The Jackson Laboratory Stock No: 007900; RRID:IMSR_JAX:007900) mice. Genotypes of interest (Cx3cr1$^{EYFP\text{-}CreER/+}$ (control) and Cx3cr1$^{EYFP\text{-}CreER/+}$:R26$^{iDTR/+}$ (experimental)) were determined by PCR using primers for R26-iDTR insertion including ROSA26-forward: AAA GTC GCT CTG AGT TGT TAT; ROSA26-reverse: GCG AAG AGT TTG TCC TCA ACC; wild-type reverse: GGA GCG GGA GAA ATG GAT ATG and primers for CreER-EYFP insertion including forward: AAG ACT CAC GTG GAC CTG CT; wild-type reverse: AGG ATG TTG ACT TCC GAG TG; mutant reverse: CGG TTA TTC AAC TTG CAC CA.

TNF knockout (referred herein as TNF KO) mice were generously supplied by Prof. Rui Applelberg (University of Porto). TNF KO mice were genotyped by PCR using ATC CGC GAC GTG GAA CTG GCA GAA (forward) and CTG CCC GGA CTC CGC AAA GTC TAA (reverse) primer pair, as before (*40*). TNF KO mice display a single band of 2 kb in the PCR gel. TNF deficient mice were generated from hemizygote progenitors, and wild-type littermates were used as controls.

Tg(Thy1-cre/ERT2,-EYFP)HGfng/PyngJ mice (also known as SLICK-H line and herein termed Thy1-YFP; The Jackson Laboratory Stock No: 012708; RRID:IMSR_JAX:012708) were maintained as before (*74*). These mice have constitutive and exclusive YFP labeling of neurons driven by the endogenous *Thy1* promoter (*75*). In this work, Thy1-YFP mice were used for studying the engulfment of synapses by microglia in vitro.

Drugs: Ethanol 99.9% (containing less than 0.0002% benzene) was obtained from Merck. Src inhibitor 1 (SKI), sulfasalazine, tamoxifen, diphtheria toxin, and rapamycin from *Streptomyces hygroscopicus* were from Sigma. AZD0530, pomalidomide and adalimumab were from Selleckchem.

Alcohol intake protocol: Mice (genotypes are specified in the Results and the Figure legends) were habituated for four weeks in experimental rooms at the i3S animal facility. Afterward, mice were randomly assigned to experimental groups.

To emulate a pattern of repetitive binge-level alcohol intake, mice were given 1.5 g/Kg ethanol (diluted to 25% in sterile tissue culture-grade water) by oral gavage daily for ten consecutive days. Vehicle control mice were gavaged with water in equal amounts to those of ethanol-gavaged mice. For analyses, mice were sacrificed 120 min after the last gavage. Animals were provided with food and water ad libitum throughout the experiments.

Measurements of blood alcohol concentration in adult C57BL/6 mice show that 120 min after oral intake of 1.5 g/Kg, around 100-120 mg/dl of ethanol is detected in their blood (*64, 65*). Based on a study by Pruett and colleagues (*76*), in which oral intake of alcohol is compared in mice and humans to achieve similar peak blood alcohol concentrations, the 1.5 g/Kg daily we used would roughly correspond to 0.83 g/Kg daily in humans, or 5 drinks a day (at 12 grams of alcohol per drink) for a person weighing 75 kg. According to the National Institute of Alcohol Abuse and Alcoholism, binge drinking is defined as five or more drinks a day for men and four or more for women (https://www.niaaa.nih.gov/alcohol-health/overview-alcohol-consumption/moderate-binge-drinking).

For in vitro studies, microglial cultures were exposed to 70 mM (320 mg/dl) ethanol. This concentration of ethanol was used because, in addition to being correlated with a dosage inducing neuronal damage (*77*) it also simulates the amounts achieved in the blood during binge drinking.

Pharmacological treatments: $Cx3cr1^{EYFP\text{-}CreER/+}$ and WT mice were subjected to a simultaneous regimen of AZD0530 (Src inhibitor; 10 mg/kg) or DMSO (control) injections (pre-treatment intraperitoneal (IP) injection followed by 5 IP injections spaced by 24 hours during the ten-day ethanol exposure regimen). The same regimen was used for the immunomodulatory agent pomalidomide (PMD; 50 mg/kg). Tamoxifen was given to adult $Cx3cr1^{EYFP\text{-}CreER/+}$ and $Cx3cr1^{EYFP\text{-}CreER/+}$:$R26^{iDTR/+}$ mice as a solution in corn oil by oral gavage. Mice received two doses of 10 mg of tamoxifen separated by 48 h between doses. For microglia ablation, 8 weeks after the last tamoxifen pulse, $Cx3cr1^{EYFP\text{-}CreER/+}$ and $Cx3cr1^{EYFP\text{-}CreER/+}$:$R26^{iDTR/+}$ mice were given diphtheria toxin (DT; 1 µg; IP) for three consecutive days and sacrifice occurred 24 h after the last DT injection.

Brain tissue preparation and immunohistochemistry: After animal perfusion with ice-cold PBS (15 ml) and fixation by perfusion with 4% PFA, brains were post-fixed by immersion in 4% PFA in PBS, pH 7.2 overnight. After that, brains were washed with PBS and then cryoprotected using sucrose gradient in a row (15 and 30%). After 24 h, brains were mounted in OCT embedding medium, frozen and cryosectioned in the CM3050S Cryostat (Leica Biosystems). Coronal sections from brains (30 µm thickness) were collected non-sequentially on Superfrost ultra plus slides. Tissue sections from controls and experimental mice encompassing identical stereological regions were collected on the same glass slide and stored at -20°C. Frozen sections were defrosted by at least 1 hour and hydrated with PBS for 15 min. Sections were permeabilized with 0.25% Triton X-100 for 15 min, washed with PBS for 10 min and blocked (5% BSA, 5% FBS, 0.1% Triton X-100) for 1 hour. Primary antibodies were incubated in a blocking solution in a humidified chamber overnight at 4°C. Secondary antibodies were incubated for 2 hours in blocking solution. After the secondary antibody, sections were washed three times for 10 min with PBS. Slides were coverslipped using glycergel or Immumount and visualized under a Leica TCS SP5 II confocal microscope.

Confocal imaging and morphometric analysis: Images from tissue sections of the prefrontal cortex and CA1 region of the dorsal hippocampus were acquired using a Leica HC PL APO Lbl. Blue 20x /0.70 IMM/CORR or a Leica HC PL APO CS 40x /1.10 CORR water objective in 8-bit sequential mode using standard TCS mode at 400 Hz and the pinhole was kept at 1 airy in the Leica TCS SP5 II confocal microscope. Images were resolved at 1024 x 1024 pixels format illuminated with 2-5% DPSS561 561 nm wave laser using a HyD detector in the BrightR mode, and entire Z-series were acquired from tissue sections. Equivalent stereological regions were acquired for all tissue sections within a given slide.

To quantify microglia, the number of YFP^+ cells was manually scored in stereological identical regions of the prefrontal cortex of stained sections (6 images per section; 5 sections per animal for each experimental group).

To quantify GFAP, the number of $GFAP^+$ cells was manually scored in stereological identical regions of the prefrontal cortex of stained sections (6 images per section; 8 sections per animal for each experimental group).

To quantify NeuN, the number of $NeuN^+$ neurons was manually scored in stereological identical regions of the prefrontal cortex stained sections (6 images per section; 8 sections per animal for each experimental group).

To quantify TNF, in brief, stereological identical regions of TNF immunostained sections of the prefrontal cortex or the dorsal hippocampal CA1 area (4 images per section; 6 sections per animal for each experimental group) were imaged, converted into 8-bit grayscale, 3D volume-rendered and thresholded. Using FIJI software, the percent of TNF immunostained area was calculated for each field, and each section.

To quantify synapses, images from stereological identical prefrontal cortex or dorsal hippocampal CA1 region from each experimental group (4 images per section; 6 sections per animal for each experimental group) were acquired using a Leica HC PL APO CS 40x /1.10 CORR water objective at 1024 x 1024 pixels resolution with 8-bit bidirectional non-sequential scanner mode at 400 Hz and pinhole at 1 airy in the Leica TCS SP5 II confocal microscope. Z-stacks were converted to maximum projection images using the LAS AF routine. Z-projections were background-subtracted using the rolling ball background subtraction built-in algorithm in FIJI, and then images were upsampled using a bicubic interpolation routine. The number of double positive PSD-95/vGlut1 puncta per μm^2 was manually scored for each image.

To quantify PSD-95 engulfment by microglia, images from stereological identical prefrontal cortex or dorsal hippocampal CA1 region from each experimental group (6 images per section; 4 sections per animal for each experimental group) were acquired using a Leica HC PL APO CS 40x /1.10 CORR water objective at 1024 x 1024 pixels

resolution with 8-bit bidirectional scanner mode at 200 Hz in the Leica TCS SP5 II confocal microscope. Using FIJI software, confocal Z stacks were background subtracted and smoothened using a Sigma filter plus. CD68, PSD-95, and Iba1 volumes were reconstructed using 3D surface rendering of confocal Z stacks in Imaris. For quantification of PSD-95 engulfment by microglia, PSD-95 puncta embedded within volume-rendered $CD68^+$ structures in $Iba1^+$ cells were considered to be engulfed by microglia. Unbiased measurements of PSD-95 puncta associated with CD68 were automatically performed using the Imaris co-localization package for each microglia and used for statistical analyses.

To assess microglial morphology, the ramification of prefrontal cortex $Iba1^+$ microglia was evaluated as described before (*78*). Branches were traced using the NeuronJ plugin, and data for each cell were converted into SWC format using Bonfire. Individual segments were connected to NeuronStudio software and audited for any tracing errors using Bonfire. Sholl analysis was performed by drawing concentric circles around the cell body at defined radius increments, separated by 6 µm. The number of intersections of branches at each defined circle was used to estimate the number of ramifications. Branching data were extracted using a custom MATLAB routine.

Flow cytometry: Mice were anesthetized and then perfused with ice-cold PBS. For single-cell suspensions, neocortices were quickly dissected on ice, placed on ice-cold RPMI, and mechanically homogenized. Cells were collected, pelleted, washed extensively, and then counted in a Neubauer chamber using trypan blue exclusion to estimate the number of live cells. Single-cell suspensions (1×10^6 cells) were incubated with different mixes of FACS antibodies for 30 min at 4°C in the dark. Compensation settings were determined using spleens from wild-type mice. Cell suspensions were evaluated on a FACS Canto II analyzer (BD Immunocytometry Systems). Microglial cell numbers found on neocortices were estimated using Precision Count Beads™ (BioLegend 424902).

Preparation of lysates and Western blotting: Cultures or mice tissues were lysed using RIPA-DTT buffer (150 mM NaCl, 50 mM Tris, 5 mM EGTA, 1% Triton X-100, 0.5% DOC, 0.1% SDS) supplemented with complete-mini protease inhibitor cocktail tablets, 1 mM DTT and phosphatase inhibitor cocktail. Samples were sonicated (6 pulses of 1 sec at 60Hz) and centrifuged at 16,000 g, 4°C for 10 min. The supernatants were collected, and the protein concentration was determined by the BCA method. All samples were denatured with sample buffer (0.5 M Tris-HCl pH 6.8, 30% glycerol, 10% SDS, 0.6 M DTT, 0.02% bromophenol blue) at 95°C for 5 min and stored at −20°C until use. Samples were separated in SDS-PAGE, transferred to PVDF membranes, which were incubated 12 hours (overnight) at 4°C with primary antibodies. Membranes were washed in TBS-T buffer pH 7.6, incubated with peroxidase-conjugated secondary antibodies and developed using an ECL chemiluminescence kit or an ECF fluorescence kit. Images were acquired in a Typhoon FLA 9000 system or ChemiDoc XRS System (Bio-Rad) and quantified by FIJI software.

Gene expression and bioinformatic analyses: RNA was extracted from neocortices using the Direct-zol™ RNA MiniPrep kit according to the manufacturer's instructions. cDNA synthesis was performed using 500 ng of total RNA (DNase I treated) with SuperScript® III First-Strand Synthesis SuperMix. qRT-PCR was carried out using iQ™ SYBR® Green Supermix on an iQ™5 multicolor real-time PCR detection system (Bio-Rad). The expression of PCR transcripts was calculated using the $2^{-deltaCt}$ with *Yhwaz* serving as the internal control gene. Statistical analyses on raw $2^{-deltaCt}$ values using unpaired *t*-tests were performed for detecting differentially expressed transcripts between sampled groups. For representation, transcript expression values were converted into Z scores. ClueGo (*79*) was used for unsupervised enrichment analyses and statistical overrepresentation of immune signaling pathways. The NetworkAnalyst 3.0 (*80*) was used for constructing topographic maps of overrepresented pathways

from gene ontology (PANTHER/SLIM GO) and for generating PPI networks (using the STRING database for the representation of interacting protein clusters).

Behavioral tests: All testing procedures were conducted in the dark phase of the light/dark cycle. Before each session, mice were removed from their home cage in the colony room and brought into the adjacent testing rooms (illuminated with 100 lux and attenuated noise). Behavioral tests were performed, as described previously (*40*), in the following order: (i) elevated plus-maze; (ii) open field; (iii) novel object recognition. The elevated plus-maze (EPM), was made of opaque grey PVC consisting of four arms arranged in a plus-shaped format; two arms have surrounding walls (closed arms, 37x6 cm x18 cm-high), while the two opposing arms have no walls (open arms, 37x6 cm). The apparatus was elevated by 50 cm above the ground. Mice were placed on the central platform facing an open arm and were allowed to explore the maze for 5 minutes. Frequency and time spent in the open arms were obtained automatically (Smart 3.0 Panlab Harvard Apparatus) and used to assess anxiety-like behavior.

For the open field (OF) test, mice were placed in the center of an OF apparatus (40 x 40 x 40 cm) and then allowed to move freely for 10 min. The total distance traveled, as well as locomotion in the peripheral zone and center zone of the apparatus were obtained automatically using video tracking.

The novel object recognition (NOR) test was performed as previously described (*81*). Briefly, the same OF test apparatus was employed, and the objects used were made of plastic, glass, or metal in three different shapes: cubes, pyramids, and cylinders. The test consists of three phases. During the habituation phase, mice are allowed to explore the apparatus for 10 min (period considered for the OF test). The following day, the acquisition/sample phase starts by placing each mouse in the apparatus with two identical objects (familiar) for 10 min. Then the mouse goes back to its home cage. After 4 hours (inter-trial interval, ITI), the retention/choice session is performed. In this phase, the apparatus contains a novel object and a copy of the last familiar object;

animals are allowed to explore these objects for 3 min. Exploration was defined as follows: mouse touched the object with its nose, or the mouse's nose was directed toward the object at a distance shorter than 2 cm (*82*). Circling or sitting on the object was not considered exploratory behavior. Behavioral data were collected using the software Observer XT 7.0, Noldus. Increased time spent exploring the novel object serves as a measure of recognition memory for the familiar object. The discrimination index (DI) was calculated as an index of memory function, DI = (time exploring the novel object - time exploring the familiar object) / (total time spent exploring both objects). Positive values indicate increased time investigating the novel object, which serves as an indication of object discrimination.

Primary cortical microglial cultures: Primary cortical microglial cell cultures were performed as previously described (*27-29, 40*). In brief, 2-day-old mouse pups were sacrificed, and their cerebral cortices were dissected in HBSS (pH 7.2) and digested with 0.07% trypsin plus 50 µL (w/v) DNAse for 15 min. The cells were gently dissociated using a glass pipette in DMEM F12 GlutaMAX™-I supplemented with 10% FBS, 0.1% gentamicin, and plated onto poly-D-lysine–coated T-flasks (75 cm^2) at $1.5x10^6$ cells per cm^2. Cultures were kept at 37°C and 95% air/5% CO_2 in a humidified incubator, and culture media was changed every 3 days for up to 21 days. To obtain purified microglial cell cultures, culture flasks were subjected to orbital shaking at 200 rpm for 2 hours. Culture supernatant was then collected into tubes, centrifuged at 453 g for 5 min at room temperature. The supernatant was discarded, and the pellet containing microglia was resuspended in culture medium. Cells were then again seeded onto poly-D-lysine–coated 6- or 12-well culture plates at 2.5 x 10^5 cells/cm^2 with DMEM F12 GlutaMAX™-I supplemented with 10% FBS, 0.1% gentamicin and 1 ng/ml GM-CSF. Purified microglia were cultured for 5 to 8 days. Immunolabeling with CD11b showed a purity of 95-99% for these cultures.

Microglial cell lines: The microglial cell line N9 was obtained by immortalization of primary cultures from the ventral mesencephalon and cerebral cortex from ED12-13 CD1 mouse embryos with the 3RV retrovirus carrying an activated v-myc oncogene (*83*). The microglial cell line CHME3 was obtained from primary cultures of human embryonic microglial cells by transfection with a plasmid encoding for the large T antigen of SV40 (*84*). Cells were cultivated and maintained as before (*27, 40*).

Synaptosomal preparations and microglia engulfment assay: To isolate prefrontal cortex synaptic terminals, synaptosomes were freshly prepared using Syn-PER™ Synaptic Protein Extraction Reagent (catalog no. 87793, ThermoFisher Scientific) precisely as recommended by the manufacturer. Briefly, WT mice or Thy1-YFP were euthanized in a CO_2 chamber. Their prefrontal cortex was collected, and homogenization was performed using a Dounce tissue grinder (~10 strokes). The homogenate was centrifuged at 1200 x *g* for 10 min, and the pellet was discarded. The supernatant was centrifuged at 15000 x *g* for 20 min. The resulting supernatant was discarded, and the synaptosomal pellet was resuspended in Syn-Per™ Synaptic Protein Extraction Reagent.

CHME3 microglial cultures were seeded in 12-well culture plates at a density of 2.5 x 10^4 cells/well in DMEM GlutaMAX™-I supplemented with 10% FBS, 0.1% PenStrep and cultivated for 48 hours. Cultures were treated with an FcγR blocking solution (1:100) for 20 min and then refed with fresh medium containing vehicle (water), or EtOH (70 mM), or adalimumab (5 μg/ml), or adalimumab (5 μg/ml) plus EtOH (70 mM). Cells were kept in those conditions for 24 hours. Afterward, cells were refed with fresh medium containing vehicle (water) plus synaptosomes (1:100), or EtOH (70 mM) plus synaptosomes (1:100), or adalimumab (5 μg/ml) plus synaptosomes (1:100), or adalimumab (5 μg/ml) plus EtOH (70 mM) plus synaptosomes (1:100). Cells were cultured under these conditions for an additional 24

hours. For analyses, microglial cultures were washed extensively with PBS and either fixed with PFA 4%, immunolabeled for PSD-95 and analyzed in a fluorescence microscope or detached using Accutase solution (catalog no. A6964, Sigma), blocked in PBS-BSA 5%, fixed with PFA 2%, resuspended in PBS-BSA 1% and analyzed in a flow cytometer.

Phagocytic assay in primary cortical microglia: Cell cultures were incubated with fluorescent latex microbeads (0.001% v/v final concentration; Sigma) for 90 min. Cultures were washed 3x with PBS and fixed in 4% PFA (w/v) for 12 min. Afterward, F-actin was stained using phalloidin, and cells were visualized in a fluorescence microscope. The number of engulfed microbeads per microglia was manually scored and plotted for statistical evaluation.

Antibodies: The following antibodies were used in this study: GFP (Abcam Cat# ab6673, RRID:AB_305643; 1:200), Iba1 (Wako Cat# 019-19741, RRID:AB_839504; 1:500), GAPDH (Hytest Cat# 5G4-9B3, RRID:AB_1616725; 1:20,000), CD11b clone M1/70.15 (BD Biosciences Cat# 560456, RRID:AB_1645267; 1:100), phospho-Src family (Tyr^{416}; Cell Signaling Technology Cat# 6943, RRID:AB_10013641; 1:100–1:200), Src clone EPR5496 (Abcam Cat# ab109381, RRID:AB_10865528; 1:1,000), PSD95 clone 6G6-1C9 (Thermo Fisher Scientific Cat# MA1-045, RRID:AB_325399; 1:600), vGlut1 (Synaptic Systems Cat# 135 303, RRID:AB_887875; 1:1,000), CD68 clone FA-11 (Bio-Rad Cat# MCA1957T, RRID:AB_2074849; 1:400), Fc Receptor Blocking Solution (BioLegend Cat# 156603, RRID:AB_2783137; 1:50), GFAP (Abcam Cat# ab7260, RRID:AB_305808; 1:100-1:500), NeuN (Millipore Cat# MAB377, RRID:AB_2298772; 1:400), APC anti-mouse/human CD11b antibody (BioLegend Cat# 101212, RRID:AB_312795; 0.25 µg to 10^6 cells), Alexa Fluor® 647 anti-mouse/human CD11b antibody (BioLegend Cat# 101218, RRID: AB_389327; 0.25 µg to 10^6 cells), PE anti-mouse CD45 antibody (BioLegend Cat#

103106, RRID:AB_312971; 0.25 µg to 10^6 cells), APC anti-mouse CD19 antibody (BioLegend Cat# 115511, RRID:AB_313646; 0.25 µg to 10^6 cells), APC/Cyanine7 anti-mouse CD3 antibody (BioLegend Cat# 100221, RRID:AB_2057374; 0.25 µg to 10^6 cells), and Brilliant Violet 421™ anti-mouse CD68 antibody (BioLegend Cat# 137017, RRID:AB_2562949; 0.25 µg to 10^6 cells).

Primers: The primers used in this study were purchased from Thermo Fisher Scientific; their sequences are provided in table S1.

Plasmids: Plasmids used in this study were purchased from Addgene: NFκB GFP–tagged p65 (RRID:Addgene_23255), IκBα-miRFP703 (RRID:Addgene_80005), pLNCX chick src Y527F (RRID:Addgene_13660), pUSE-RapR-Src-myc (RRID:Addgene_25933), psPAX2 (RRID:Addgene_12260), pMD2.G (RRID:Addgene_12259), pUMVC (RRID:Addgene_8449), pMSCV (RRID:Addgene_24828), and pCherry-FRB (RRID:Addgene_25920).

Retroviruses production: Low-passage HEK293T cells were seeded in 100 mm culture dishes. When cultures reached ~80% confluence cells were co-transfected overnight with viruses-producing plasmids using the transfection reagent jetPRIME®. Transfection ratios were as follows: 6 µg of shRNA plasmids to 3 µg of psPAX2 to 3 µg of VSVG (2:1:1) for lentiviruses production or 8 µg of Src^{Y527F} construct to 4 µg of pUMVC to 2 µg of VSVG (4:2:1) for viral production. The next day, normal growth media replaced transfection media, and cells were cultivated for an additional 48 hours. Next, media with viral particles were collected, centrifuged at 906 g for 15 min at 4°C, and the supernatant was collected into new tubes and kept at -80°C.

Live cell imaging and FRET: Microglial cells were plated on plastic-bottom culture dishes (µ-Dish 35 mm, iBidi). Imaging was performed using a Leica DMI6000B inverted

microscope. The excitation light source was a mercury metal halide bulb integrated with an EL6000 light attenuator. High-speed, low vibration external filter wheels (equipped with CFP/YFP/farRed excitation and emission filters) were mounted on the microscope (Fast Filter Wheels, Leica Microsystems). A 440-520nm dichroic mirror (CG1, Leica Microsystems) and a PlanApo 63X 1.3NA glycerol immersion objective were used for CFP and FRET images. Images were acquired with 2x2 binning using a digital CMOS camera (ORCA-Flash4.0 V2, Hamamatsu Photonics). At each time-point, CFP, FRET, and fared images were sequentially acquired using different filter combinations. (*27-29, 40*). For quantifications, images were exported as 16-bit tiff files and processed in FIJI software. The background was dynamically subtracted from all frames from both channels. Segmentation (on a pixel-by-pixel basis) and generation of 32-bit float-point ratiometric images were achieved using the precision FRET (PFRET) data processing software package for ImageJ (https://lvg.virginia.edu/digital-downloads/pfret-data-processing-software). The mean gray intensity values from ratio images were used for statistical calculations.

Cytokine release: Culture medium was collected to tubes and centrifuged at 16,000 g at 4°C for 5 min. The supernatant was transferred to a new tube and kept at -80°C. The concentration of TNF in cell culture supernatants was quantified by enzyme-linked immunosorbent assay (ELISA) following the instructions provided by the manufacturer (Peprotech, UK). Absorbance at 405 nm, with wavelength correction at 650 nm, was measured with a multimode microplate reader (Synergy HT, Biotek, USA). Values corresponding to ng/ml were obtained by extrapolating a standard concentration curve using recombinant TNF.

Statistics: A 95% confidence interval was used for statistical evaluation, and $P < 0.05$ was considered a statistically significant difference in all sampled groups. Experimental units in individual replicates were prior evaluated for Gaussian distribution using the

D'Agostino & Pearson omnibus normality test with GraphPad Prism. When comparing only two experimental groups, a Mann-Whitney test for data with non-normal distribution or an unpaired Student's *t*-test with equal variance assumption for data with normal distribution was used. When comparing three to four independent conditions, a one-way ANOVA followed by the Sidak's multiple comparisons test was used. When comparing treatment effects within genotypes or mutants, a two-way ANOVA followed by the Sidak's multiple comparisons test was used. Two-way ANOVA was also used to compare values of microglia intersections retrieved from Sholl analysis. To minimize bias, experimental groups were assigned through randomization. Specifically, sampled groups evaluated in Figures 1 and 2, and all supplementary figures were assigned using "simple random sampling". Sampled assessed groups in Figures 3 through 7 were assigned using "permuted block randomization". All quantifications were performed blinded.

Supplementary Materials

Figure S1. Alcohol exposure does not activate other resident immune cells in the neocortex.

Figure S2. Alcohol exposure modulates microglial TNF production through a Src–NF-κB pathway.

Figure S3. Alcohol exposure does not alter general locomotor activity or recognition memory.

Figure S4. Alcohol induces synapse loss without affecting neuronal numbers.

Figure S5. Alcohol exposure does not alter synapse number, postsynaptic engulfment, or TNF production in the CA1 region of the dorsal hippocampus.

Table S1. Primers.

References and Notes

1. D. M. Lovinger, M. Roberto, Synaptic effects induced by alcohol. *Current topics in behavioral neurosciences* **13**, 31-86 (2013)10.1007/7854_2011_143).

2. K. P. Abrahao, A. G. Salinas, D. M. Lovinger, Alcohol and the Brain: Neuronal Molecular Targets, Synapses, and Circuits. *Neuron* **96**, 1223-1238 (2017); published online EpubDec 20 (10.1016/j.neuron.2017.10.032).

3. M. J. Lacagnina, P. D. Rivera, S. D. Bilbo, Glial and Neuroimmune Mechanisms as Critical Modulators of Drug Use and Abuse. *Neuropsychopharmacology : official publication of the American College of Neuropsychopharmacology* **42**, 156-177 (2017); published online EpubJan (10.1038/npp.2016.121).

4. M. Prinz, D. Erny, N. Hagemeyer, Ontogeny and homeostasis of CNS myeloid cells. *Nature immunology* **18**, 385-392 (2017); published online EpubMar 22 (10.1038/ni.3703).

5. A. Crotti, R. M. Ransohoff, Microglial Physiology and Pathophysiology: Insights from Genome-wide Transcriptional Profiling. *Immunity* **44**, 505-515 (2016); published online EpubMar 15 (10.1016/j.immuni.2016.02.013).

6. M. W. Salter, B. Stevens, Microglia emerge as central players in brain disease. *Nature medicine* **23**, 1018-1027 (2017); published online EpubSep 08 (10.1038/nm.4397).

7. A. Vilalta, G. C. Brown, Neurophagy, the phagocytosis of live neurons and synapses by glia, contributes to brain development and disease. *The FEBS journal* **285**, 3566-3575 (2018).

8. J. He, F. T. Crews, Increased MCP-1 and microglia in various regions of the human alcoholic brain. *Exp Neurol* **210**, 349-358 (2008).

9. J. Y. Yang, X. Xue, H. Tian, X. X. Wang, Y. X. Dong, F. Wang, Y. N. Zhao, X. C. Yao, W. Cui, C. F. Wu, Role of microglia in ethanol-induced neurodegenerative disease: Pathological and behavioral dysfunction at different developmental stages. *Pharmacology & therapeutics* **144**, 321-337 (2014); published online EpubDec (10.1016/j.pharmthera.2014.07.002).

10. C. Cui, D. Shurtleff, R. A. Harris, Neuroimmune mechanisms of alcohol and drug addiction. *International review of neurobiology* **118**, 1-12 (2014)10.1016/b978-0-12-801284-0.00001-4).

11. J. Mayfield, L. Ferguson, R. A. Harris, Neuroimmune signaling: a key component of alcohol abuse. *Current opinion in neurobiology* **23**, 513-520 (2013).

12. J. F. Henriques, C. C. Portugal, T. Canedo, J. B. Relvas, T. Summavielle, R. Socodato, Microglia and alcohol meet at the crossroads: Microglia as critical modulators of alcohol neurotoxicity. *Toxicology letters* **283**, 21-31 (2018); published online EpubFeb (10.1016/j.toxlet.2017.11.002).

13. A. Warden, E. Erickson, G. Robinson, R. A. Harris, R. D. Mayfield, The neuroimmune transcriptome and alcohol dependence: potential for targeted therapies. *Pharmacogenomics* **17**, 2081-2096 (2016); published online EpubDec (10.2217/pgs-2016-0062).

14. E. K. Erickson, E. K. Grantham, A. S. Warden, R. A. Harris, Neuroimmune signaling in alcohol use disorder. *Pharmacology, biochemistry, and behavior* **177**, 34-60 (2019); published online EpubFeb (10.1016/j.pbb.2018.12.007).

15. L. Qin, F. T. Crews, NADPH oxidase and reactive oxygen species contribute to alcohol-induced microglial activation and neurodegeneration. *Journal of neuroinflammation* **9**, 5 (2012); published online EpubJan 12 (10.1186/1742-2094-9-5).

16. C. N. Parkhurst, G. Yang, I. Ninan, J. N. Savas, J. R. Yates, 3rd, J. J. Lafaille, B. L. Hempstead, D. R. Littman, W. B. Gan, Microglia promote learning-dependent synapse formation through brain-derived neurotrophic factor. *Cell* **155**, 1596-1609 (2013); published online EpubDec 19 (10.1016/j.cell.2013.11.030).

17. S. Alfonso-Loeches, J. R. Urena-Peralta, M. J. Morillo-Bargues, J. Oliver-De La Cruz, C. Guerri, Role of mitochondria ROS generation in ethanol-induced NLRP3 inflammasome activation and cell death in astroglial cells. *Frontiers in cellular neuroscience* **8**, 216 (2014)10.3389/fncel.2014.00216).

18. M. Pascual-Lucas, S. Fernandez-Lizarbe, J. Montesinos, C. Guerri, LPS or ethanol triggers clathrin- and rafts/caveolae-dependent endocytosis of TLR4 in cortical astrocytes. *Journal of neurochemistry* **129**, 448-462 (2014); published online EpubMay (10.1111/jnc.12639).

19. R. Minambres, R. M. Guasch, A. Perez-Arago, C. Guerri, The RhoA/ROCK-I/MLC pathway is involved in the ethanol-induced apoptosis by anoikis in astrocytes. *Journal of cell science* **119**, 271-282 (2006); published online EpubJan 15 (10.1242/jcs.02723).

20. S. L. Valles, A. M. Blanco, M. Pascual, C. Guerri, Chronic ethanol treatment enhances inflammatory mediators and cell death in the brain and in astrocytes. *Brain pathology (Zurich, Switzerland)* **14**, 365-371 (2004); published online EpubOct (10.1111/j.1750-3639.2004.tb00079.x).

21. A. Pla, M. Pascual, C. Guerri, Autophagy Constitutes a Protective Mechanism against Ethanol Toxicity in Mouse Astrocytes and Neurons. *PloS one* **11**, e0153097 (2016)10.1371/journal.pone.0153097).

22. A. M. Blanco, S. L. Valles, M. Pascual, C. Guerri, Involvement of TLR4/type I IL-1 receptor signaling in the induction of inflammatory mediators and cell death induced by ethanol in cultured astrocytes. *Journal of immunology (Baltimore, Md. : 1950)* **175**, 6893-6899 (2005); published online EpubNov 15 (10.4049/jimmunol.175.10.6893).

23. T. J. Walter, F. T. Crews, Microglial depletion alters the brain neuroimmune response to acute binge ethanol withdrawal. *Journal of neuroinflammation* **14**, 86 (2017); published online EpubApr 20 (10.1186/s12974-017-0856-z).

24. G. W. Muller, R. Chen, S. Y. Huang, L. G. Corral, L. M. Wong, R. T. Patterson, Y. Chen, G. Kaplan, D. I. Stirling, Amino-substituted thalidomide analogs: potent inhibitors of TNF-alpha production. *Bioorganic & medicinal chemistry letters* **9**, 1625-1630 (1999); published online EpubJun 7 (

25. C. Galustian, B. Meyer, M. C. Labarthe, K. Dredge, D. Klaschka, J. Henry, S. Todryk, R. Chen, G. Muller, D. Stirling, P. Schafer, J. B. Bartlett, A. G. Dalgleish, The anti-cancer agents lenalidomide and pomalidomide inhibit the proliferation and function of T regulatory cells. *Cancer immunology, immunotherapy : CII* **58**, 1033-1045 (2009); published online EpubJul (10.1007/s00262-008-0620-4).

26. Z. Li, Y. Qiu, D. Personett, P. Huang, B. Edenfield, J. Katz, D. Babusis, Y. Tang, M. A. Shirely, M. F. Moghaddam, J. A. Copland, H. W. Tun, Pomalidomide shows significant therapeutic activity against CNS lymphoma with a major impact on the tumor microenvironment in murine models. *PloS one* **8**, e71754 (2013)10.1371/journal.pone.0071754).

27. C. C. Portugal, R. Socodato, T. Canedo, C. M. Silva, T. Martins, V. S. Coreixas, E. C. Loiola, B. Gess, D. Rohr, A. R. Santiago, P. Young, R. D. Minshall, R. Paes-de-Carvalho, A. F. Ambrosio, J. B. Relvas, Caveolin-1-mediated internalization of the vitamin C transporter SVCT2 in microglia triggers an inflammatory phenotype. *Science signaling* **10**, (2017); published online EpubMar 28 (10.1126/scisignal.aal2005).

28. R. Socodato, C. C. Portugal, T. Canedo, I. Domith, N. A. Oliveira, R. Paes-de-Carvalho, J. B. Relvas, M. Cossenza, c-Src deactivation by the polyphenol 3-O-caffeoylquinic acid abrogates reactive oxygen species-mediated glutamate release from microglia and neuronal excitotoxicity. *Free Radic Biol Med* **79**, 45-55 (2015); published online EpubFeb (10.1016/j.freeradbiomed.2014.11.019).

29. R. Socodato, C. C. Portugal, I. Domith, N. A. Oliveira, V. S. Coreixas, E. C. Loiola, T. Martins, A. R. Santiago, R. Paes-de-Carvalho, A. F. Ambrosio, J. B. Relvas, c-Src function is necessary and sufficient for triggering microglial cell activation. *Glia* **63**, 497-511 (2015); published online EpubMar (10.1002/glia.22767).

30. S. Zhao, J. Yin, L. Zhou, F. Yan, Q. He, L. Huang, S. Peng, J. Jia, J. Cheng, H. Chen, W. Tao, X. Ji, Y. Xu, Z. Yuan, Hippo/MST1 signaling mediates microglial activation following acute cerebral ischemia–reperfusion injury. *Brain, Behavior, and Immunity* **55**, 236-248 (2016); published online Epub2016/07/01/ (https://doi.org/10.1016/j.bbi.2015.12.016).

31. A. C. Kaufman, S. V. Salazar, L. T. Haas, J. Yang, M. A. Kostylev, A. T. Jeng, S. A. Robinson, E. C. Gunther, C. H. van Dyck, H. B. Nygaard, S. M. Strittmatter, Fyn inhibition rescues established memory and synapse loss in Alzheimer mice. *Annals of neurology* **77**, 953-971 (2015); published online EpubJun (10.1002/ana.24394).

32. T. Liu, L. Zhang, D. Joo, S.-C. Sun, NF-κB signaling in inflammation. *Signal transduction and targeted therapy* **2**, 17023 (2017).

33. G. Bonizzi, M. Karin, The two NF-κB activation pathways and their role in innate and adaptive immunity. *Trends in immunology* **25**, 280-288 (2004).

34. D. M. Shcherbakova, M. Baloban, A. V. Emelyanov, M. Brenowitz, P. Guo, V. V. Verkhusha, Bright monomeric near-infrared fluorescent proteins as tags and biosensors for multiscale imaging. *Nature Communications* **7**, 12405 (2016); published online Epub08/19/online (10.1038/ncomms12405 https://www.nature.com/articles/ncomms12405#supplementary-information).

35. A. V. Karginov, F. Ding, P. Kota, N. V. Dokholyan, K. M. Hahn, Engineered allosteric activation of kinases in living cells. *Nat Biotechnol* **28**, 743-747 (2010).

36. H. T. Gan, Y. Q. Chen, Q. Ouyang, Sulfasalazine inhibits activation of nuclear factor-kappaB in patients with ulcerative colitis. *Journal of gastroenterology and hepatology* **20**, 1016-1024 (2005); published online EpubJul (10.1111/j.1440-1746.2005.03862.x).

37. C. K. Weber, S. Liptay, T. Wirth, G. Adler, R. M. Schmid, Suppression of NF-kappaB activity by sulfasalazine is mediated by direct inhibition of IkappaB kinases alpha and beta. *Gastroenterology* **119**, 1209-1218 (2000); published online EpubNov (

38. R. C. Froemke, Plasticity of cortical excitatory-inhibitory balance. *Annual review of neuroscience* **38**, 195-219 (2015).

39. R. Tatti, M. S. Haley, O. K. Swanson, T. Tselha, A. Maffei, Neurophysiology and regulation of the balance between excitation and inhibition in neocortical circuits. *Biological psychiatry* **81**, 821-831 (2017).

40. R. Socodato, C. C. Portugal, T. Canedo, A. Rodrigues, T. O. Almeida, J. F. Henriques, S. H. Vaz, J. Magalhães, C. M. Silva, F. I. Baptista, R. L. Alves, V. Coelho-Santos, A. P. Silva, R. Paes-de-Carvalho, A. Magalhães, C. Brakebusch, A. M. Sebastião, T. Summavielle, A. F. Ambrósio, J. B. Relvas, Microglia Dysfunction Caused by the Loss of Rhoa Disrupts Neuronal Physiology and Leads to Neurodegeneration. *Cell Rep* **31**, 107796 (2020); published online EpubJun 23 (10.1016/j.celrep.2020.107796).

41. P. Ayata, A. Badimon, H. J. Strasburger, M. K. Duff, S. E. Montgomery, Y.-H. E. Loh, A. Ebert, A. A. Pimenova, B. R. Ramirez, A. T. Chan, Epigenetic regulation of brain region-specific microglia clearance activity. *Nature neuroscience* **21**, 1049 (2018).

42. C. J. Kane, P. D. Drew, Inflammatory responses to alcohol in the CNS: nuclear receptors as potential therapeutics for alcohol-induced neuropathologies. *Journal of leukocyte biology* **100**, 951-959 (2016); published online EpubNov (10.1189/jlb.3MR0416-171R).

43. J. Montesinos, S. Alfonso-Loeches, C. Guerri, Impact of the Innate Immune Response in the Actions of Ethanol on the Central Nervous System. *Alcoholism, clinical and experimental research* **40**, 2260-2270 (2016); published online EpubNov (10.1111/acer.13208).

44. F. T. Crews, R. Bechara, L. A. Brown, D. M. Guidot, P. Mandrekar, S. Oak, L. Qin, G. Szabo, M. Wheeler, J. Zou, Cytokines and alcohol. *Alcoholism: Clinical and Experimental Research* **30**, 720-730 (2006).

45. N. M. Zahr, K. L. Kaufman, C. G. Harper, Clinical and pathological features of alcohol-related brain damage. *Nature Reviews Neurology* **7**, 284 (2011).

46. S. Alfonso-Loeches, M. Pascual-Lucas, A. Blanco, I. Sanchez-Vera, C. Guerri, Pivotal role of TLR4 receptors in alcohol-induced neuroinflammation and brain damage. *The Journal of neuroscience: the official journal of the Society for Neuroscience* **30**, 8285 (2010).

47. D. Lippai, S. Bala, T. Csak, E. A. Kurt-Jones, G. Szabo, Chronic alcohol-induced microRNA-155 contributes to neuroinflammation in a TLR4-dependent manner in mice. *PloS one* **8**, e70945 (2013).

48. D. Lippai, S. Bala, J. Petrasek, T. Csak, I. Levin, E. A. Kurt-Jones, G. Szabo, Alcohol-induced IL-1β in the brain is mediated by NLRP3/ASC inflammasome activation that amplifies neuroinflammation. *Journal of leukocyte biology* **94**, 171-182 (2013).

49. J. Liu, J. M. Lewohl, P. R. Dodd, P. K. Randall, R. A. Harris, R. D. Mayfield, Gene expression profiling of individual cases reveals consistent transcriptional changes in alcoholic human brain. *Journal of neurochemistry* **90**, 1050-1058 (2004); published online EpubSep (10.1111/j.1471-4159.2004.02570.x).

50. J. Liu, J. M. Lewohl, R. A. Harris, V. R. Iyer, P. R. Dodd, P. K. Randall, R. D. Mayfield, Patterns of gene expression in the frontal cortex discriminate alcoholic from nonalcoholic individuals. *Neuropsychopharmacology : official publication of the American College of Neuropsychopharmacology* **31**, 1574-1582 (2006); published online EpubJul (10.1038/sj.npp.1300947).

51. R. D. Mayfield, J. M. Lewohl, P. R. Dodd, A. Herlihy, J. Liu, R. A. Harris, Patterns of gene expression are altered in the frontal and motor cortices of human alcoholics. *Journal of neurochemistry* **81**, 802-813 (2002); published online EpubMay (10.1046/j.1471-4159.2002.00860.x).

52. M. K. Mulligan, I. Ponomarev, R. J. Hitzemann, J. K. Belknap, B. Tabakoff, R. A. Harris, J. C. Crabbe, Y. A. Blednov, N. J. Grahame, T. J. Phillips, D. A. Finn, P. L. Hoffman, V. R. Iyer, G. F. Koob, S. E. Bergeson, Toward understanding the genetics of alcohol drinking through transcriptome meta-analysis. *Proceedings of the National Academy of Sciences of the United States of America* **103**, 6368-6373 (2006); published online EpubApr 18 (10.1073/pnas.0510188103).

53. E. Osterndorff-Kahanek, I. Ponomarev, Y. A. Blednov, R. A. Harris, Gene expression in brain and liver produced by three different regimens of alcohol consumption in mice: comparison with immune activation. *PloS one* **8**, e59870 (2013)10.1371/journal.pone.0059870).

54. G. M. McCarthy, S. P. Farris, Y. A. Blednov, R. A. Harris, R. D. Mayfield, Microglial-specific transcriptome changes following chronic alcohol consumption. *Neuropharmacology* **128**, 416-424 (2018); published online EpubJan (10.1016/j.neuropharm.2017.10.035).

55. A. Dolganiuc, G. Bakis, K. Kodys, P. Mandrekar, G. Szabo, Acute ethanol treatment modulates Toll-like receptor-4 association with lipid rafts.

Alcoholism, clinical and experimental research **30**, 76-85 (2006); published online EpubJan (10.1111/j.1530-0277.2006.00003.x).

56. S. Oak, P. Mandrekar, D. Catalano, K. Kodys, G. Szabo, TLR2- and TLR4-mediated signals determine attenuation or augmentation of inflammation by acute alcohol in monocytes. *Journal of immunology (Baltimore, Md. : 1950)* **176**, 7628-7635 (2006); published online EpubJun 15 (10.4049/jimmunol.176.12.7628).

57. M. Pang, S. Bala, K. Kodys, D. Catalano, G. Szabo, Inhibition of TLR8- and TLR4-induced Type I IFN induction by alcohol is different from its effects on inflammatory cytokine production in monocytes. *BMC immunology* **12**, 55 (2011); published online EpubSep 30 (10.1186/1471-2172-12-55).

58. P. Mandrekar, S. Bala, D. Catalano, K. Kodys, G. Szabo, The opposite effects of acute and chronic alcohol on lipopolysaccharide-induced inflammation are linked to IRAK-M in human monocytes. *Journal of immunology (Baltimore, Md. : 1950)* **183**, 1320-1327 (2009); published online EpubJul 15 (10.4049/jimmunol.0803206).

59. M. Manukyan, P. Nalbant, S. Luxen, K. M. Hahn, U. G. Knaus, RhoA GTPase activation by TLR2 and TLR3 ligands: connecting via Src to NF-kappa B. *Journal of immunology (Baltimore, Md. : 1950)* **182**, 3522-3529 (2009); published online EpubMar 15 (10.4049/jimmunol.0802280).

60. S. Biswas, A. Zimman, D. Gao, T. V. Byzova, E. A. Podrez, TLR2 Plays a Key Role in Platelet Hyperreactivity and Accelerated Thrombosis Associated With Hyperlipidemia. *Circulation research* **121**, 951-962 (2017); published online EpubSep 29 (10.1161/circresaha.117.311069).

61. I. T. Lee, S. W. Wang, C. W. Lee, C. C. Chang, C. C. Lin, S. F. Luo, C. M. Yang, Lipoteichoic acid induces HO-1 expression via the TLR2/MyD88/c-Src/NADPH oxidase pathway and Nrf2 in human tracheal smooth muscle cells. *Journal of immunology (Baltimore, Md. : 1950)* **181**, 5098-5110 (2008); published online EpubOct 1 (10.4049/jimmunol.181.7.5098).

62. M. Wolfl, S. Schwinn, Y. E. Yoo, M. L. Ress, M. Braun, M. Chopra, S. C. Schreiber, V. I. Ayala, C. Ohlen, M. Eyrich, A. Beilhack, P. G. Schlegel, Src-kinase inhibitors sensitize human cells of myeloid origin to Toll-like-receptor-induced interleukin 12 synthesis. *Blood* **122**, 1203-1213 (2013); published online EpubAug 15 (10.1182/blood-2013-03-488072).

63. B. Haider, A. Duque, A. R. Hasenstaub, D. A. McCormick, Neocortical network activity in vivo is generated through a dynamic balance of excitation and inhibition. *The Journal of neuroscience : the official journal of the Society for Neuroscience* **26**, 4535-4545 (2006); published online EpubApr 26 (10.1523/jneurosci.5297-05.2006).

64. N. Y. Golovenko, M. S. Zhuk, V. G. Zin'kovskii, O. V. Zhuk, M. V. Kopanitsa, Pharmacokinetics of Ethanol in Mice with Different Alcohol Motivation. *Bulletin of Experimental Biology and Medicine* **132**, 852-855 (2001); published online EpubSeptember 01 (10.1023/a:1013166601027).

65. J. C. Crabbe, C. J. Cotnam, A. J. Cameron, J. P. Schlumbohm, J. S. Rhodes, P. Metten, D. Wahlsten, Strain differences in three measures of ethanol

intoxication in mice: the screen, dowel and grip strength tests. *Genes, brain, and behavior* **2**, 201-213 (2003); published online EpubAug (

66. J. P. ter Horst, E. R. de Kloet, H. Schächinger, M. S. Oitzl, Relevance of Stress and Female Sex Hormones for Emotion and Cognition. *Cellular and Molecular Neurobiology* **32**, 725-735 (2012); published online Epub2012/07/01 (10.1007/s10571-011-9774-2).

67. A. Villa, P. Gelosa, L. Castiglioni, M. Cimino, N. Rizzi, G. Pepe, F. Lolli, E. Marcello, L. Sironi, E. Vegeto, A. Maggi, Sex-Specific Features of Microglia from Adult Mice. *Cell Rep* **23**, 3501-3511 (2018)10.1016/j.celrep.2018.05.048).

68. M. Pascual, J. Montesinos, M. Marcos, J.-L. Torres, P. Costa-Alba, F. García-García, F.-J. Laso, C. Guerri, Gender differences in the inflammatory cytokine and chemokine profiles induced by binge ethanol drinking in adolescence. *Addict Biol* **22**, 1829-1841 (2017)10.1111/adb.12461).

69. S. Alfonso-Loeches, M. Pascual, C. Guerri, Gender differences in alcohol-induced neurotoxicity and brain damage. *Toxicology* **311**, 27-34 (2013)10.1016/j.tox.2013.03.001).

70. L. Weinhard, G. di Bartolomei, G. Bolasco, P. Machado, N. L. Schieber, U. Neniskyte, M. Exiga, A. Vadisiute, A. Raggioli, A. Schertel, Y. Schwab, C. T. Gross, Microglia remodel synapses by presynaptic trogocytosis and spine head filopodia induction. *Nature Communications* **9**, 1228 (2018); published online Epub2018/03/26 (10.1038/s41467-018-03566-5).

71. A. R. Aroor, R. C. Baker, Ethanol inhibition of phagocytosis and superoxide anion production by microglia. *Alcohol (Fayetteville, N.Y.)* **15**, 277-280 (1998); published online EpubMay (10.1016/s0741-8329(97)00129-8).

72. L. Gofman, J. M. Cenna, R. Potula, P2X4 receptor regulates alcohol-induced responses in microglia. *Journal of neuroimmune pharmacology : the official journal of the Society on NeuroImmune Pharmacology* **9**, 668-678 (2014); published online EpubDec (10.1007/s11481-014-9559-8).

73. S. Kalinin, M. Gonzalez-Prieto, H. Scheiblich, L. Lisi, H. Kusumo, M. T. Heneka, J. L. M. Madrigal, S. C. Pandey, D. L. Feinstein, Transcriptome analysis of alcohol-treated microglia reveals downregulation of beta amyloid phagocytosis. *Journal of neuroinflammation* **15**, 141 (2018); published online EpubMay 14 (10.1186/s12974-018-1184-7).

74. C. Karabiyik, R. Fernandes, F. R. Figueiredo, R. Socodato, C. Brakebusch, K. L. Lambertsen, J. B. Relvas, S. D. Santos, Neuronal Rho GTPase Rac1 elimination confers neuroprotection in a mouse model of permanent ischemic stroke. *Brain Pathology* **28**, 569-580 (2018).

75. P. Young, L. Qiu, D. Wang, S. Zhao, J. Gross, G. Feng, Single-neuron labeling with inducible Cre-mediated knockout in transgenic mice. *Nature neuroscience* **11**, 721-728 (2008)10.1038/nn.2118).

76. S. Pruett, W. Tan, G. E. Howell, 3rd, B. Nanduri, Dosage Scaling of Alcohol in Binge Exposure Models in Mice: An Empirical Assessment of the Relationship Between Dose, Alcohol Exposure, and Peak Blood

Concentrations in Humans and Mice. *Alcohol*, (2020); published online EpubApr 4 (10.1016/j.alcohol.2020.03.011).

77. C. Ikonomidou, P. Bittigau, M. J. Ishimaru, D. F. Wozniak, C. Koch, K. Genz, M. T. Price, V. Stefovska, F. Hörster, T. Tenkova, K. Dikranian, J. W. Olney, Ethanol-Induced Apoptotic Neurodegeneration and Fetal Alcohol Syndrome. *Science* **287**, 1056 (2000)10.1126/science.287.5455.1056).

78. C. G. Langhammer, M. L. Previtera, E. S. Sweet, S. S. Sran, M. Chen, B. L. Firestein, Automated Sholl analysis of digitized neuronal morphology at multiple scales: whole cell Sholl analysis versus Sholl analysis of arbor subregions. *Cytometry Part A* **77**, 1160-1168 (2010).

79. G. Bindea, B. Mlecnik, H. Hackl, P. Charoentong, M. Tosolini, A. Kirilovsky, W.-H. Fridman, F. Pagès, Z. Trajanoski, J. Galon, ClueGO: a Cytoscape plug-in to decipher functionally grouped gene ontology and pathway annotation networks. *Bioinformatics* **25**, 1091-1093 (2009)10.1093/bioinformatics/btp101).

80. G. Zhou, O. Soufan, J. Ewald, R. E. W. Hancock, N. Basu, J. Xia, NetworkAnalyst 3.0: a visual analytics platform for comprehensive gene expression profiling and meta-analysis. *Nucleic acids research* **47**, W234-w241 (2019); published online EpubJul 2 (10.1093/nar/gkz240).

81. M. Leger, A. Quiedeville, V. Bouet, B. Haelewyn, M. Boulouard, P. Schumann-Bard, T. Freret, Object recognition test in mice. *Nature protocols* **8**, 2531-2537 (2013); published online EpubDec (10.1038/nprot.2013.155).

82. A. Ennaceur, S. Michalikova, A. Bradford, S. Ahmed, Detailed analysis of the behavior of Lister and Wistar rats in anxiety, object recognition and object location tasks. *Behavioural brain research* **159**, 247-266 (2005); published online EpubApr 30 (10.1016/j.bbr.2004.11.006).

83. M. Righi, L. Mori, G. De Libero, M. Sironi, A. Biondi, A. Mantovani, S. D. Donini, P. Ricciardi-Castagnoli, Monokine production by microglial cell clones. *Eur J Immunol* **19**, 1443-1448 (1989); published online EpubAug (10.1002/eji.1830190815).

84. N. Janabi, S. Peudenier, B. Heron, K. H. Ng, M. Tardieu, Establishment of human microglial cell lines after transfection of primary cultures of embryonic microglial cells with the SV40 large T antigen. *Neurosci Lett* **195**, 105-108 (1995); published online EpubAug 4 (

Acknowledgments: The authors acknowledge the support of the following i3S Scientific Platforms: Animal Facility, Cell Culture and Genotyping (CCGen), Translational Cytometry Unit (TraCy), and Advanced Light Microscopy (ALM), member of the national infrastructure PPBI-Portuguese Platform of BioImaging (POCI-01–0145-FEDER-022122). The authors also acknowledge Prof. Rui Applelberg for generously supplying TNF KO mice. **Funding:** This work was financed by FEDER - Fundo Europeu de Desenvolvimento Regional funds through the COMPETE 2020 - Operacional Programme for Competitiveness and Internationalisation (POCI), Portugal 2020, and by Portuguese funds through FCT - Fundação para a Ciência e a Tecnologia/Ministério da Ciência, Tecnologia e Ensino Superior in the framework of the project POCI-01-0145-FEDER-030647 (PTDC/SAU-TOX/30647/2017) in TS lab. The projects FEDER Portugal (Norte-01-0145-FEDER-000008000008—Porto Neurosciences and Neurologic Disease Research Initiative at I3S, supported by Norte Portugal Regional Operational Programme (NORTE 2020), under the PORTUGAL 2020 Partnership Agreement, through the European Regional Development Fund (ERDF); FCOMP-01-0124-FEDER-021333) and FCT (PTDC/MED-NEU/31318/2017) supported work in JBR lab. CCP and RS hold employment contracts financed by national funds through FCT – Fundação para a Ciência e a Tecnologia, I.P., in the context of the program-contract described in paragraphs 4, 5 and 6 of art. 23 of Law no. 57/2016, of August 29, as amended by Law no. 57/2017 of July 2019. TC is supported by FCT (SFRH/BD/117148/2016). RLA was supported by FCT (PD/BD/114266/2016). AM was supported by FCT (IF/00753/2014). **Author contributions:** RS, TS, and JBR designed the project. RS, JFH, CCP, TOA, JTM, RLA, TC, CS, and AM performed experiments. RS, TS, and JBR co-supervised the study. RS and JBR wrote the original draft. RS, CCP, TS, and JBR reviewed and edited the manuscript. TS and JBR acquired funding. **Competing interests:** The authors declare that they have no competing interests. **Data and materials availability:** All

data needed to evaluate the conclusions in the paper are present in the paper or the Supplementary Materials.

Figure Legends

Figure 1. Alcohol intake elicits microglia activation in the prefrontal cortex. (A) Schematic of the regimen of repetitive binge-level alcohol (EtOH) intake to adult Cx3cr1$^{EYFP\text{-}CreER/+}$ mice. Mice were given EtOH (1.5 g/Kg) or water (H_2O; control) by oral gavage for ten consecutive days. **(B)** Histological confocal analysis of microglia (immunostained against YFP) on tissue sections from prefrontal cortices of Cx3cr1$^{EYFP\text{-}CreER/+}$ mice exposed to EtOH or H_2O. Asterisks indicate the microglial cell body. Scale bar: 50 µm. Data are mean ± SEM from 6 mice per condition pooled across 3 independent experiments. *P<0.05 by Mann-Whitney test. **(C)** Flow cytometry analysis of microglial numbers in neocortices of Cx3cr1$^{EYFP\text{-}CreER/+}$ mice exposed to EtOH or H_2O. Microglia were identified as being CD11b^{+} and Cd45$^{low/mid}$ gated from the double-positive CD11b^{+} YFP^{+} population. Data are mean ± SEM from 8 (H_2O) and 9 (EtOH) mice pooled across 3 independent experiments. *P<0.05 by Mann-Whitney test. **(D)** Western blot for Iba1 on lysates from prefrontal cortices of Cx3cr1$^{EYFP\text{-}CreER/+}$ mice exposed to EtOH or H_2O. GAPDH (loading control). Data are mean ± SEM from 6 mice per condition pooled across 3 independent experiments. *P<0.05 by Mann-Whitney test. **(E)** Sholl analysis retrieved from histological confocal images of Iba1 on tissue sections from prefrontal cortices of Cx3cr1$^{EYFP\text{-}CreER/+}$ mice exposed to EtOH or H_2O (n=50 cells from 5 animals per group for each distance). Scale bar: 20 µm. Data are mean ± SEM from 50 cells for each distance from 5 mice per condition pooled across 3 independent experiments. *P<0.05 by two-way ANOVA with Sidak's multiple comparisons. **(F)** qRT-PCR from neocortices of Cx3cr1$^{EYFP\text{-}CreER/+}$ mice exposed to EtOH or H_2O. The clustered histogram shows the Z scores of mRNA transcripts

normalized to the H_2O values. Data are mean ± SEM from 5 mice per condition pooled across 3 independent experiments. *P<0.05 by Mann-Whitney test. **(G)** Pathway enrichment analysis inputting the transcripts shown in (F). Graphs show the top 10 most overrepresented ontology terms in the GO biological process and the Reactome pathways.

Figure 2. Alcohol intake triggers a TNF-associated neuroimmune response. (A and B) qRT-PCR from neocortices of $Cx3cr1^{EYFP\text{-}CreER/+}$ mice exposed to EtOH or H_2O. The clustered histogram shows the Z scores of mRNA transcripts normalized to the H_2O values. Transcripts differentially altered by EtOH are shown in (A); those not significantly altered by EtOH are shown in (B). Data are means ± SEM from 5 mice per condition pooled across 3 independent experiments. *P<0.05 by Mann-Whitney test. **(C)** Pathway enrichment analysis inputting the transcripts shown in A. The topographic pathway map shows overrepresented (orange) and underrepresented (purple) terms (nodes) and their degree of interaction (gray lines). Color ramps display the significance enrichment of each node. All nodes shown in the map are associated directly or indirectly with TNF signaling. **(D)** String-based protein-protein interaction (PPI) networks constructed inputting the transcripts shown in (A). Protein clusters that were significantly modulated by EtOH are color-coded based on their degree of association and significance, as indicated.

Figure 3. TNF production elicited by alcohol intake drives microglia activation in the prefrontal cortex. (A) Schematic of tamoxifen-inducible microglial ablation in the brain from postnatal day 28 (P28). Tamox, tamoxifen; DT, diphtheria toxin. **(B)** Histological confocal analysis for Iba1 on tissue sections from prefrontal cortices of $Cx3cr1^{EYFP\text{-}CreER/+}$ and $Cx3cr1^{EYFP\text{-}CreER/+}$:$R26^{iDTR/+}$ after exposure to diphtheria toxin

(DT; n=4 animals per genotype). Scale bar: 50 µm. **(C)** Flow cytometry analysis of microglial numbers in neocortices of Cx3cr1$^{EYFP\text{-}CreER/+}$ and Cx3cr1$^{EYFP\text{-}CreER/+}$:R26$^{iDTR/+}$ after exposure to DT. Data are mean ± SEM from 6 mice per condition pooled across 3 independent experiments. *P<0.05 by Mann-Whitney test. **(D)** Schematic of microglial ablation during EtOH exposure. **(E)** qRT-PCR from neocortices of Cx3cr1$^{EYFP\text{-}CreER/+}$ and Cx3cr1$^{EYFP\text{-}CreER/+}$:R26$^{iDTR/+}$ after microglia ablation during exposure to EtOH or H_2O. Histogram shows the Z scores of TNF transcripts normalized to the Cx3cr1$^{EYFP\text{-}CreER/+}$ - H_2O values. Data are mean ± SEM from 5 mice per condition pooled across 3 independent experiments. *P<0.05 by two-way ANOVA with Sidak's multiple comparisons. **(F)** Histological confocal analysis for TNF on tissue sections from prefrontal cortices of Cx3cr1$^{EYFP\text{-}CreER/+}$ and Cx3cr1$^{EYFP\text{-}CreER/+}$:R26$^{iDTR/+}$ after microglia ablation during exposure to EtOH or H_2O. Scale bar: 100 µm. Data are mean ± SEM from 5 mice per condition pooled across 3 independent experiments. *P<0.05 by two-way ANOVA with Sidak's multiple comparisons. **(G)** Flow cytometry analysis of microglial numbers in neocortices of wild-type (WT) or TNF knockout (KO) mice exposed to EtOH or H_2O. WT animals were also treated with DMSO or with pomalidomide (PMD). Data are mean ± SEM from at least 8 mice per condition pooled across 3 independent experiments. *P<0.05 by two-way ANOVA with Sidak's multiple comparisons. **(H)** qRT-PCR from neocortices of WT or TNF KO mice exposed to EtOH or H_2O. Histogram shows the Z scores of mRNA transcripts normalized to the WT - H_2O values. Data are mean ± SEM from 5 mice per condition pooled across 3 independent experiments. *P<0.05 by two-way ANOVA with Sidak's multiple comparisons.

Figure 4. Src activation elicited by alcohol intake leads to TNF production driving prefrontal cortex microglia activation. (A) Western blot analysis for Src phospho-Tyr^{416} (active form) on lysates from prefrontal cortices of Cx3cr1$^{EYFP\text{-}CreER/+}$ and Cx3cr1$^{EYFP\text{-}CreER/+}$:R26$^{iDTR/+}$ after microglia ablation during exposure to EtOH or H_2O. Src (loading control). Data are mean ± SEM from 5 mice per condition pooled across 3 independent experiments. *P<0.05 by two-way ANOVA with Sidak's multiple comparisons. **(B)** qRT-PCR from neocortices of Cx3cr1$^{EYFP\text{-}CreER/+}$ mice exposed to EtOH or H_2O. Mice were treated with either DMSO or the brain-penetrant Src inhibitor AZD0530. Data are mean ± SEM from 5 mice per condition pooled across 3 independent experiments. *P<0.05 by two-way ANOVA with Sidak's multiple comparisons. **(C)** CHME3 microglial cultures expressing Src or control shRNA were transfected with a GFP-tagged p65 NFkB subunit (p65-GFP) construct and were treated for 24 hours with EtOH (70 mM) or H_2O. Scale bar: 10 μm. Data are mean ± SEM from 8 independent cultures per condition. *P<0.05 by one-way ANOVA with Sidak's multiple comparisons. **(D)** N9 microglial cultures expressing an empty pMSCV vector (EV) or the Src^{Y527F} mutant were treated with 1 mM sulfasalazine for 24 h and immunostained for TNF and CD11b. TNF fluorescence intensity per individual microglia in each cell culture is coded according to the indicated pseudocolor scale. Scale bar: 20 μm. Data are mean ± SEM from at least 4 independent cultures per condition. *P<0.05 by one-way ANOVA with Sidak's multiple comparisons. **(E)** Flow cytometry analysis of microglial numbers in neocortices of Cx3cr1$^{EYFP\text{-}CreER/+}$ mice exposed to EtOH or H_2O. Mice were treated with either DMSO or AZD0530. Data are mean ± SEM from 8 mice per condition pooled across 3 independent experiments. *P<0.05 by two-way ANOVA with Sidak's multiple comparisons. **(F)** qRT-PCR from neocortices of Cx3cr1$^{EYFP\text{-}CreER/+}$ mice exposed to EtOH or H_2O. Mice were also treated with DMSO or with AZD0530. The clustered histogram shows the Z scores of mRNA transcripts normalized to the DMSO - H_2O values. Data are mean ± SEM from 5 mice

per condition pooled across 3 independent experiments. *P<0.05 by two-way ANOVA with Sidak's multiple comparisons.

Figure 5. Alcohol intake elicits anxiety-like behavior in a microglia-dependent manner. (A and B) Cx3cr1$^{EYFP\text{-}CreER/+}$ mice were injected with DMSO, AZD0530, or PMD and exposed to EtOH or H_2O and then evaluated in the elevated-plus maze (EPM) test. Data are mean ± SEM from at least 9 mice per condition pooled across at least from 3 independent experiments. *P<0.05 by two-way ANOVA with Sidak's multiple comparisons. **(C and D)** Cx3cr1$^{EYFP\text{-}CreER/+,}$ and Cx3cr1$^{EYFP\text{-}CreER/+}$:R26$^{iDTR/+}$ mice were given tamoxifen, treated with diphtheria toxin to ablate microglia during exposure to EtOH or H_2O, and then evaluated in the EPM. Data are mean ± SEM from 6 mice per condition pooled across 3 independent experiments. *P<0.05 by two-way ANOVA with Sidak's multiple comparisons.

Figure 6. Alcohol intake elicits synapse loss in a microglia-dependent manner. (A) Confocal imaging analysis for PSD-95 (red) and vGlut1 (green) on tissue sections from prefrontal cortices of WT and TNF KO mice after exposure to EtOH or H_2O. Scale bar: 5 μm. Data are mean ± SEM from at least 6 mice per condition pooled across 3 independent experiments. ****P<0.0001 and ***P<0.001 by two-way ANOVA with Sidak's multiple comparisons. **(B)** Confocal imaging analysis for PSD-95 (red) and vGlut1 (green) on tissue sections from prefrontal cortices of in Cx3cr1$^{EYFP\text{-}CreER/+}$ and Cx3cr1$^{EYFP\text{-}CreER/+}$:R26$^{iDTR/+}$ mice after microglia ablation during exposure to EtOH or H_2O. Scale bar: 5 μm. Data are mean ± SEM from at least 6 mice per condition pooled across 3 independent experiments. ****P<0.0001 and ***P<0.001 by two-way ANOVA with Sidak's multiple comparisons. **(C)** Western blot analysis for PSD-95 and vGlut1 on lysates from prefrontal cortices of Cx3cr1$^{EYFP\text{-}CreER/+}$ and Cx3cr1$^{EYFP\text{-}CreER/+}$:R26$^{iDTR/+}$

mice after microglia ablation during exposure to EtOH or H_2O. GAPDH (loading control). Data are mean ± SEM from 5 mice per condition pooled across 3 independent experiments. *P<0.05 by two-way ANOVA with Sidak's multiple comparisons.

Figure 7. Alcohol intake enables microglia to prune synapses. (A) Representative Imaris 3D surface rendering of confocal maximum projection images showing volume reconstruction of PSD-95 within CD68 structures in microglia ($Iba1^+$ cell) on tissue sections from prefrontal cortices of WT and TNF KO mice after exposure to EtOH or H_2O. Scale bar: 5 μm. Data are mean ± SEM from 12 microglia per condition derived from 4 mice pooled across 3 independent experiments. *P<0.05 by two-way ANOVA with Sidak's multiple comparisons. **(B)** Immunofluorescence images of PSD-95-labeled prefrontal cortex synaptosomes (red) inside cultured CHME3 microglia labeled with CellMask dye (blue). Scale bar: 20 μm. Data are mean ± SEM from 62 cells per condition from 3 independent experiments. *P<0.05 by unpaired *t*-test. **(C)** Representative flow cytometry profiles for YFP labeling in CHME3 microglia incubated for 24 hours with synaptosomes isolated from the prefrontal cortex of Thy1-YFP mice. In some conditions, microglial cultures were pretreated for 24 hours with EtOH (70 mM) or with the TNF blocking antibody adalimumab (5 μg/ml). Engulfment ability of microglia was calculated by comparing the percentage (left graph) or the normalized MFIs (right graph) of microglia expressing a high YFP signal. Data are mean ± SEM from 6 independent experiments per condition. *P<0.05 by two-way ANOVA with Sidak's multiple comparisons. **(D)** qRT-PCR from neocortices of WT and TNF KO mice exposed to EtOH or H_2O. The clustered histogram shows the Z scores of mRNA transcripts normalized to the DMSO - H_2O values. Data are mean ± SEM from 5 mice per condition pooled across 3 independent experiments. *P<0.05 by two-way ANOVA with Sidak's multiple comparisons. **(E)** Flow cytometry analysis of CD68 expression in microglia (gated as $CD45^{mid}CD11b^+$ cell population) from prefrontal cortices of

$Cx3cr1^{EYFP\text{-}CreER/+}$ mice exposed to EtOH or H_2O. Data are mean ± SEM from 5 mice per condition pooled across 3 independent experiments. *P<0.05 by two-way ANOVA with Sidak's multiple comparisons. **(F)** Primary cortical microglial cultures were treated with EtOH (70 mM) or H_2O, incubated with fluorescent microbeads (green) for 90 min and stained with phalloidin (red). Scale bar: 20 µm. Data are mean ± SEM from 4 independent experiments per condition. *P<0.05 by two-way ANOVA with Sidak's multiple comparisons.

Figure 1.

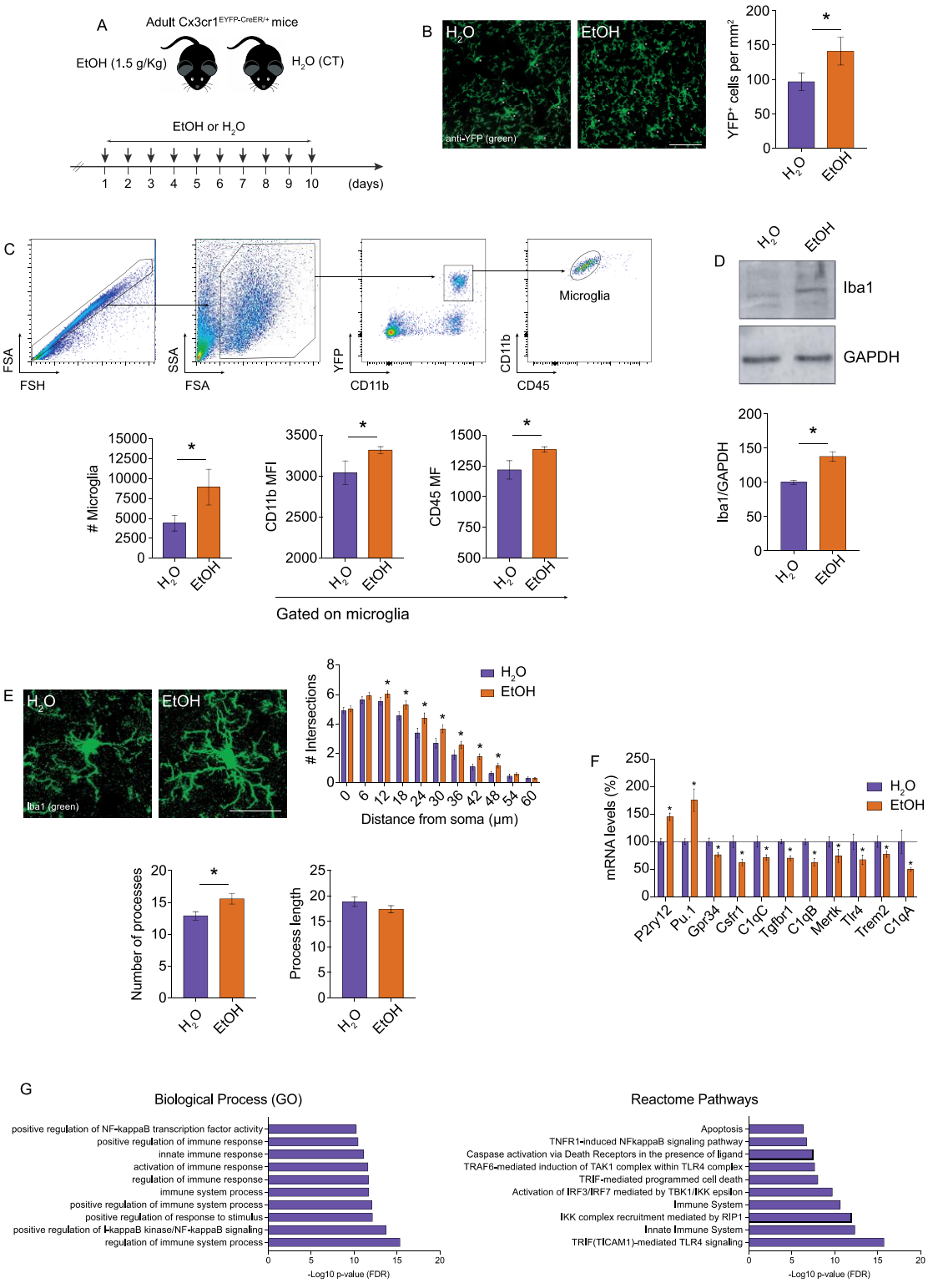
A
Adult Cx3cr1EYFP-CreER/+ mice
EtOH (1.5 g/Kg)
H2O (CT)
EtOH or H2O
1 2 3 4 5 6 7 8 9 10 (days)
B
H2O
EtOH
anti-YFP (green)
YFP+ cells per mm2
C
FSA
FSH
SSA
FSA
YFP
CD11b
CD11b
CD45
Microglia
Microglia
CD11b MFI
CD45 MF
Gated on microglia
D
H2O
EtOH
Iba1
GAPDH
Iba1/GAPDH
E
H2O
EtOH
Iba1 (green)
Intersections
Distance from soma (µm)
Number of processes
Process length
F
mRNA levels (%)
P2ry12
Pu.1
Gpr34
Csfr1
C1qC
Tgfbr1
C1qB
Mertk
Tlr4
Trem2
C1qA
G
Biological Process (GO)
positive regulation of NF-kappaB transcription factor activity
positive regulation of immune response
innate immune response
activation of immune response
regulation of immune response
immune system process
positive regulation of immune system process
positive regulation of response to stimulus
positive regulation of I-kappaB kinase/NF-kappaB signaling
regulation of immune system process
-Log10 p-value (FDR)
Reactome Pathways
Apoptosis
TNFR1-induced NFkappaB signaling pathway
Caspase activation via Death Receptors in the presence of ligand
TRAF6-mediated induction of TAK1 complex within TLR4 complex
TRIF-mediated programmed cell death
Activation of IRF3/IRF7 mediated by TBK1/IKK epsilon
Immune System
IKK complex recruitment mediated by RIP1
Innate Immune System
TRIF(TICAM1)-mediated TLR4 signaling
-Log10 p-value (FDR)

Figure 2.

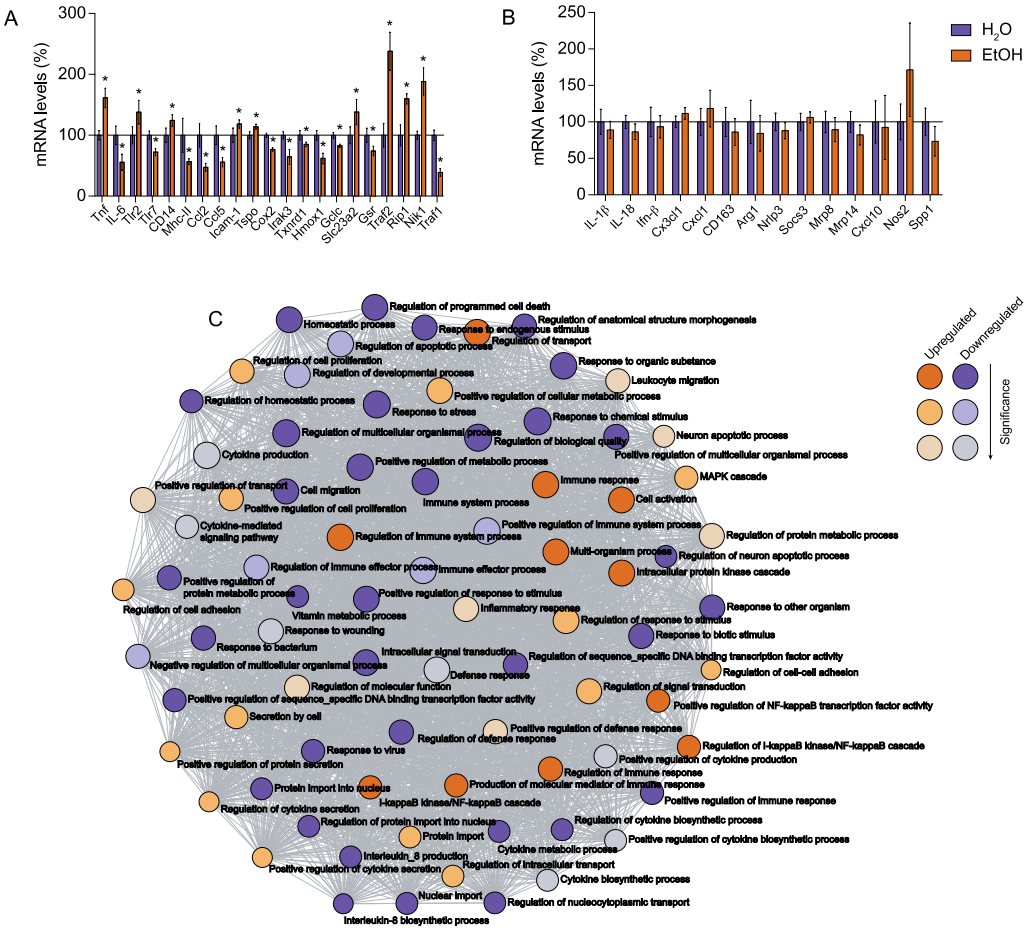
A
mRNA levels (%)
300
200
100
0
Tnf
IL-6
Tlr2
Tlr7
CD14
Mhc-II
Ccl2
Ccl5
Icam-1
Tspo
Cox2
Irak3
Txnrd1
Hmox1
Gclc
Slc23a2
Gsr
Traf2
Rip1
Nlk1
Traf1
B
mRNA levels (%)
250
200
150
100
50
0
H2O
EtOH
IL-1β
IL-18
Ifn-β
Cx3cl1
Cxcl1
CD163
Arg1
Nrlp3
Socs3
Mrp8
Mrp14
Cxcl10
Nos2
Spp1
C
Regulation of programmed cell death
Homeostatic process
Regulation of anatomical structure morphogenesis
Response to endogenous stimulus
Regulation of apoptotic process
Regulation of transport
Regulation of cell proliferation
Regulation of developmental process
Response to organic substance
Leukocyte migration
Regulation of homeostatic process
Positive regulation of cellular metabolic process
Response to stress
Response to chemical stimulus
Regulation of multicellular organismal process
Regulation of biological quality
Neuron apoptotic process
Cytokine production
Positive regulation of multicellular organismal process
Positive regulation of metabolic process
Immune response
MAPK cascade
Positive regulation of transport
Cell migration
Immune system process
Cell activation
Positive regulation of cell proliferation
Cytokine-mediated signaling pathway
Regulation of immune system process
Positive regulation of immune system process
Regulation of protein metabolic process
Multi-organism process
Regulation of neuron apoptotic process
Regulation of immune effector process
Immune effector process
Intracellular protein kinase cascade
Positive regulation of protein metabolic process
Positive regulation of response to stimulus
Regulation of cell adhesion
Inflammatory response
Response to other organism
Vitamin metabolic process
Regulation of response to stimulus
Response to wounding
Response to biotic stimulus
Response to bacterium
Intracellular signal transduction
Regulation of sequence_specific DNA binding transcription factor activity
Negative regulation of multicellular organismal process
Defense response
Regulation of cell-cell adhesion
Regulation of molecular function
Regulation of signal transduction
Positive regulation of sequence_specific DNA binding transcription factor activity
Positive regulation of NF-kappaB transcription factor activity
Secretion by cell
Positive regulation of defense response
Regulation of defense response
Regulation of I-kappaB kinase/NF-kappaB cascade
Response to virus
Positive regulation of cytokine production
Positive regulation of protein secretion
Regulation of immune response
Protein import into nucleus
Production of molecular mediator of immune response
I-kappaB kinase/NF-kappaB cascade
Positive regulation of immune response
Regulation of cytokine secretion
Regulation of protein import into nucleus
Regulation of cytokine biosynthetic process
Protein import
Cytokine metabolic process
Positive regulation of cytokine biosynthetic process
Interleukin_8 production
Positive regulation of cytokine secretion
Regulation of intracellular transport
Cytokine biosynthetic process
Nuclear import
Regulation of nucleocytoplasmic transport
Interleukin-8 biosynthetic process
Upregulated
Downregulated
Significance
D
Tlr2
Tspo
Tlr7
Ccl2
Irak3
Ccl5
Icam1
Tnf
Gclc
Hmox1
Casp1
Tyk2
Rhoa
Rac1
Cav1
Lyn
Hck
Cd68
Fyn
Jak2
Lck
Fgr
Tnfrsf1b
Notch1
Src
Nfkbia
Nfkbie
Casp3
Adam10
Casp8
Traf2
Csf1
Adam17
Ikbkg
Casp9
Lamp2
Rela
Tnfrsf1a
Lamp1
Hdac4
Ptn cluster
Degree of interaction
Ptn network
Degree of overlap

Figure 3.

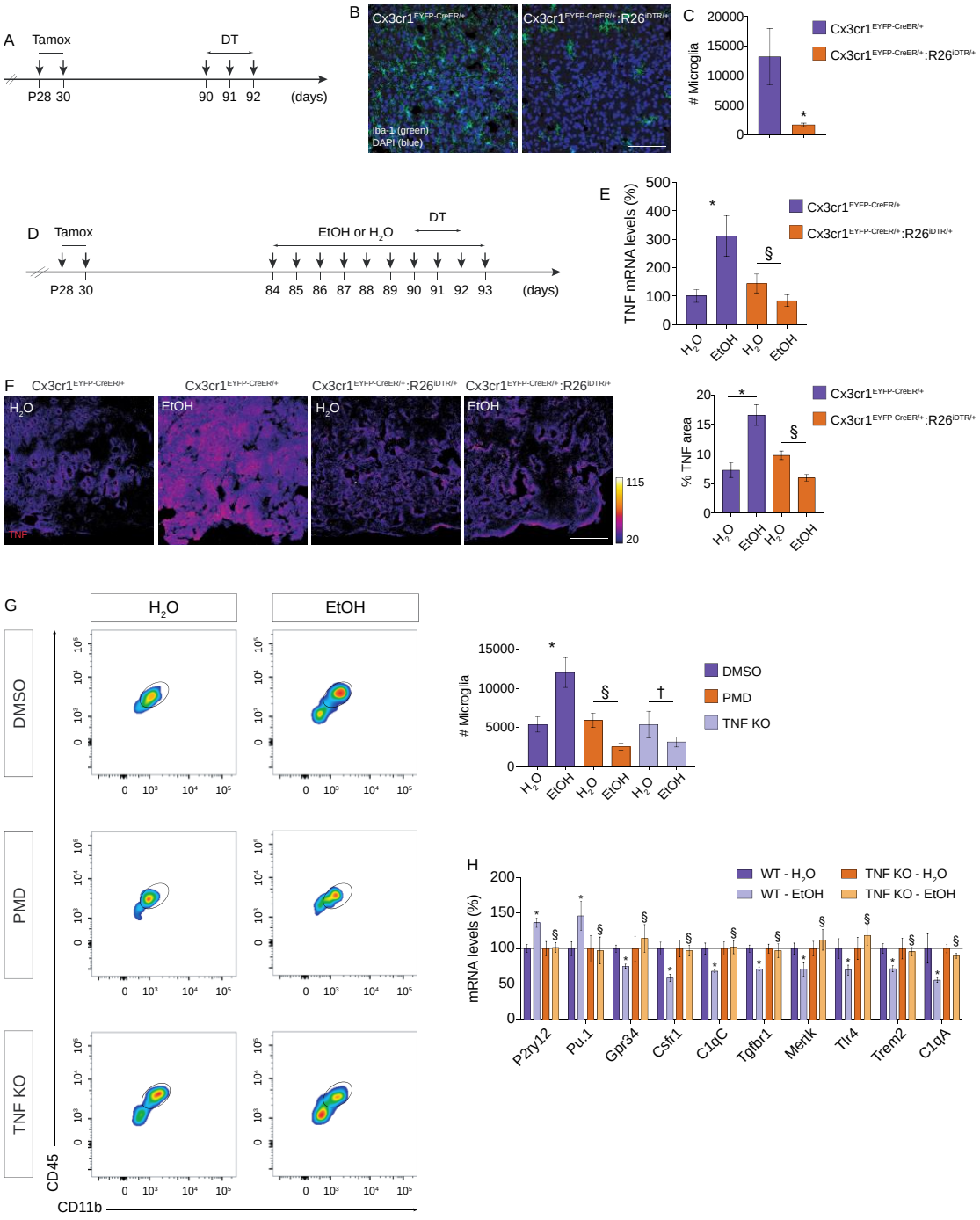
A
Tamox
DT
P28 30
90 91 92
(days)
B
Cx3cr1EYFP-CreER/+
Cx3cr1EYFP-CreER/+:R26iDTR/+
Iba-1 (green)
DAPI (blue)
C
Microglia
20000
15000
10000
5000
0
Cx3cr1EYFP-CreER/+
Cx3cr1EYFP-CreER/+:R26iDTR/+
D
Tamox
EtOH or H2O
DT
P28 30
84 85 86 87 88 89 90 91 92 93
(days)
E
TNF mRNA levels (%)
500
400
300
200
100
0
H2O
EtOH
F
Cx3cr1EYFP-CreER/+
Cx3cr1EYFP-CreER/+:R26iDTR/+
TNF
115
20
% TNF area
20
15
10
5
0
G
H2O
EtOH
DMSO
PMD
TNF KO
CD45
CD11b
Microglia
15000
10000
5000
0
DMSO
PMD
TNF KO
H
mRNA levels (%)
200
150
100
50
0
WT - H2O
WT - EtOH
TNF KO - H2O
TNF KO - EtOH
P2ry12
Pu.1
Gpr34
Csfr1
C1qC
Tgfbr1
Mertk
Tlr4
Trem2
C1qA

Figure 4.

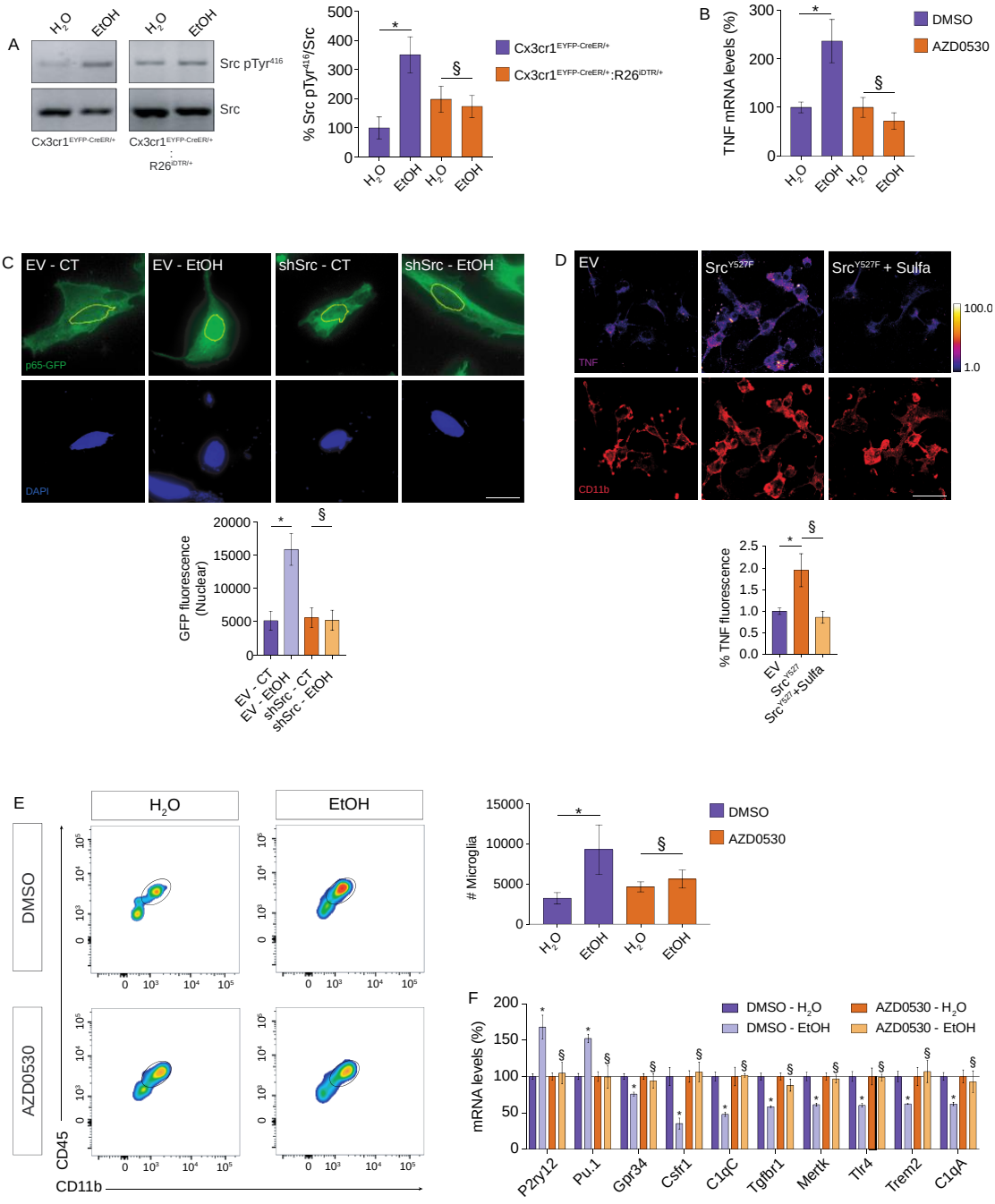
A
H2O
EtOH
H2O
EtOH
Src pTyr416
Src
Cx3cr1EYFP-CreER/+
Cx3cr1EYFP-CreER/+ : R26iDTR/+
% Src pTyr416/Src
Cx3cr1EYFP-CreER/+
Cx3cr1EYFP-CreER/+:R26iDTR/+
B
TNF mRNA levels (%)
DMSO
AZD0530
C
EV - CT
EV - EtOH
shSrc - CT
shSrc - EtOH
p65-GFP
DAPI
GFP fluorescence (Nuclear)
D
EV
SrcY527F
SrcY527F + Sulfa
TNF
CD11b
% TNF fluorescence
E
H2O
EtOH
DMSO
AZD0530
CD45
CD11b
Microglia
F
DMSO - H2O
DMSO - EtOH
AZD0530 - H2O
AZD0530 - EtOH
mRNA levels (%)
P2ry12
Pu.1
Gpr34
Csfr1
C1qC
Tgfbr1
Mertk
Tlr4
Trem2
C1qA

Figure 5.

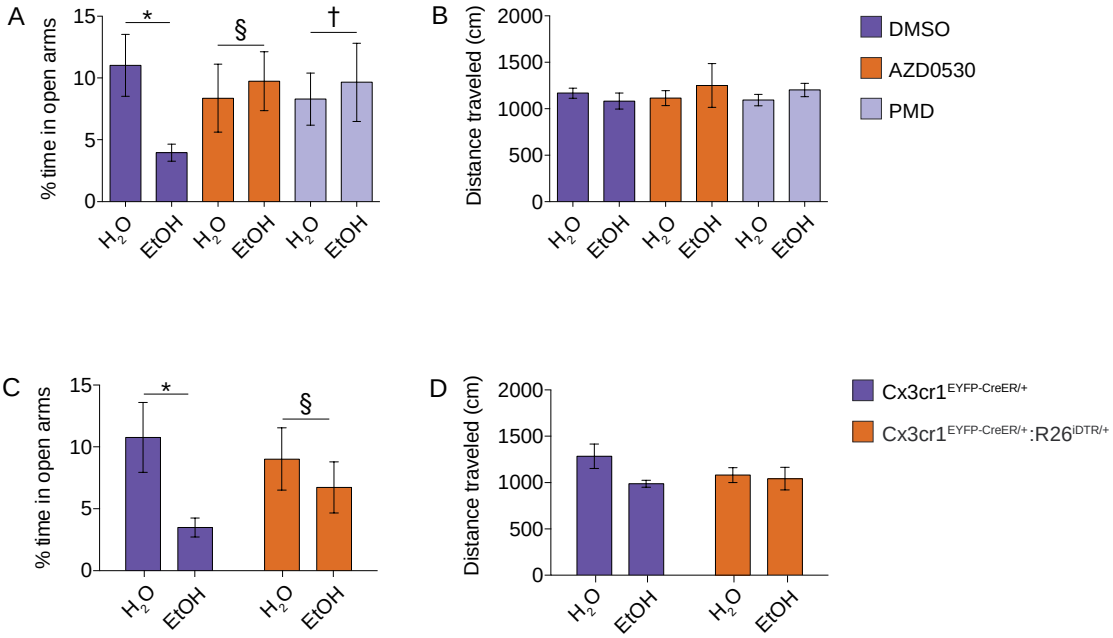
A
% time in open arms
15
10
5
0
*
§
†
H2O
EtOH
B
Distance traveled (cm)
2000
1500
1000
500
0
DMSO
AZD0530
PMD
C
% time in open arms
*
§
D
Distance traveled (cm)
Cx3cr1EYFP-CreER/+
Cx3cr1EYFP-CreER/+:R26iDTR/+

Figure 6.

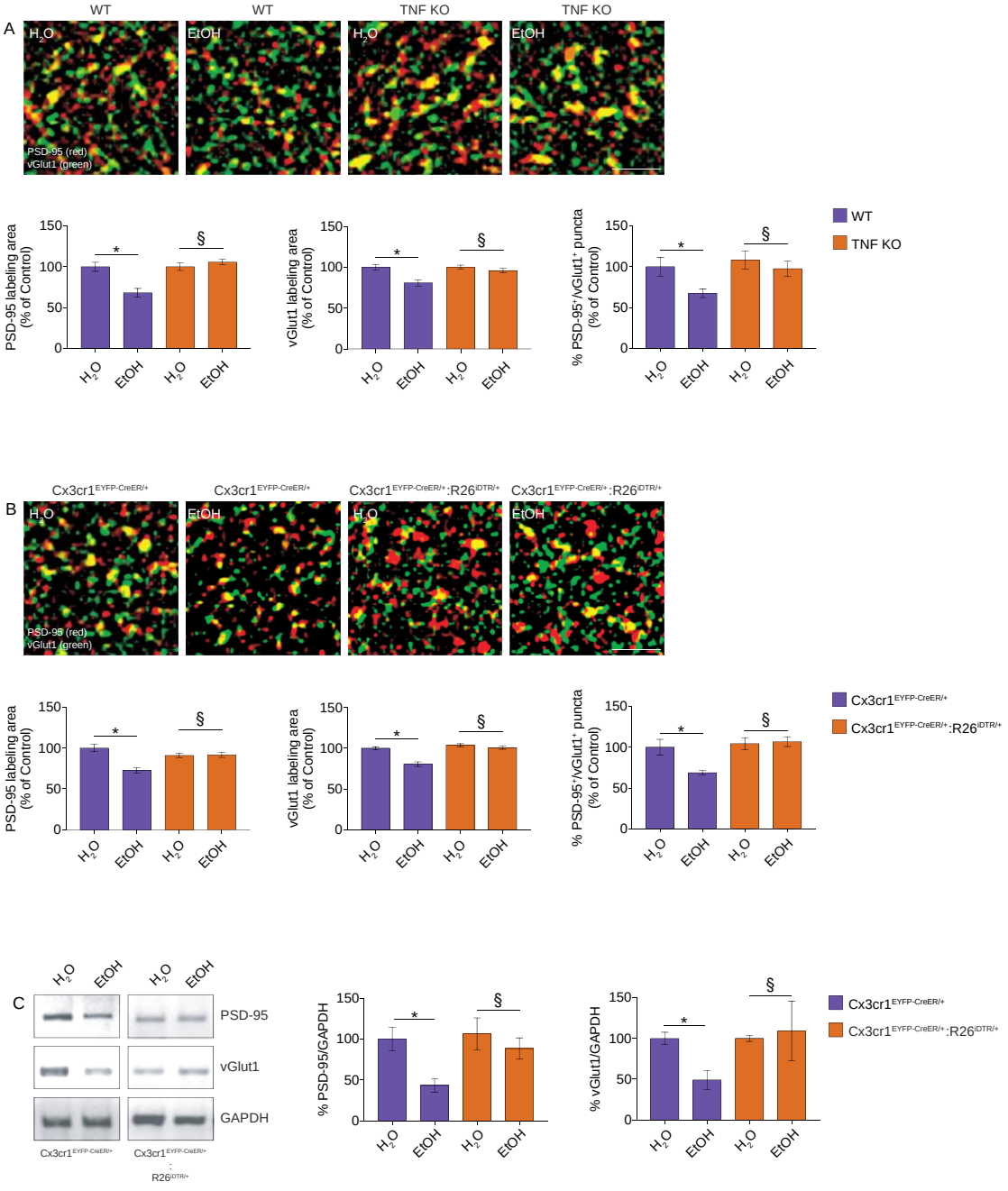
A
WT
WT
TNF KO
TNF KO
H2O
EtOH
H2O
EtOH
PSD-95 (red)
vGlut1 (green)
PSD-95 labeling area (% of Control)
vGlut1 labeling area (% of Control)
% PSD-95+/vGlut1+ puncta (% of Control)
H2O
EtOH
H2O
EtOH
WT
TNF KO
B
Cx3cr1EYFP-CreER/+
Cx3cr1EYFP-CreER/+
Cx3cr1EYFP-CreER/+:R26iDTR/+
Cx3cr1EYFP-CreER/+:R26iDTR/+
H2O
EtOH
H2O
EtOH
PSD-95 (red)
vGlut1 (green)
PSD-95 labeling area (% of Control)
vGlut1 labeling area (% of Control)
% PSD-95+/vGlut1+ puncta (% of Control)
Cx3cr1EYFP-CreER/+
Cx3cr1EYFP-CreER/+:R26iDTR/+
C
H2O
EtOH
H2O
EtOH
PSD-95
vGlut1
GAPDH
Cx3cr1EYFP-CreER/+
Cx3cr1EYFP-CreER/+ : R26iDTR/+
% PSD-95/GAPDH
% vGlut1/GAPDH
Cx3cr1EYFP-CreER/+
Cx3cr1EYFP-CreER/+:R26iDTR/+

Figure 7.

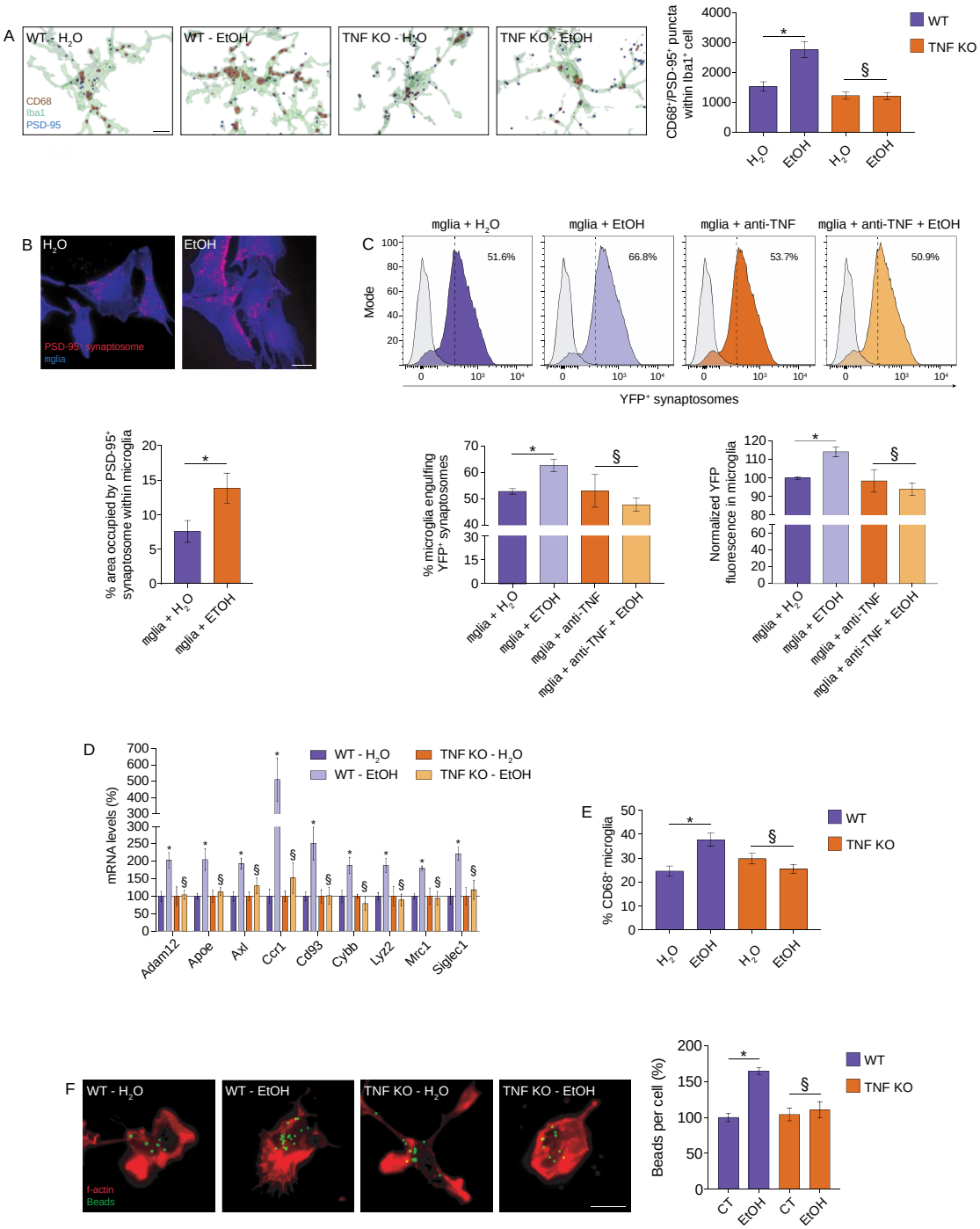

SUPPLEMENTARY MATERIALS

http://stke.sciencemag.org/cgi/content/full/13/650/eaba5754/DC1

Supplementary Materials for

Daily alcohol intake triggers aberrant synaptic pruning leading to synapse loss and anxiety-like behavior

Renato Socodato*, Joana F. Henriques, Camila C. Portugal, Tiago O. Almeida, Joana Tedim-Moreira, Renata L. Alves, Teresa Canedo, Cátia Silva, Ana Magalhães, Teresa Summavielle*, João B. Relvas*

*Corresponding author. Email: renato.socodato@ibmc.up.pt (R.S.); tsummavi@ibmc.up.pt (T.S.); jrelvas@ibmc.up.pt (J.B.R.)

Published 22 September 2020, *Sci. Signal.* **13**, eaba5754 (2020)
DOI: 10.1126/scisignal.aba5754

This PDF file includes:

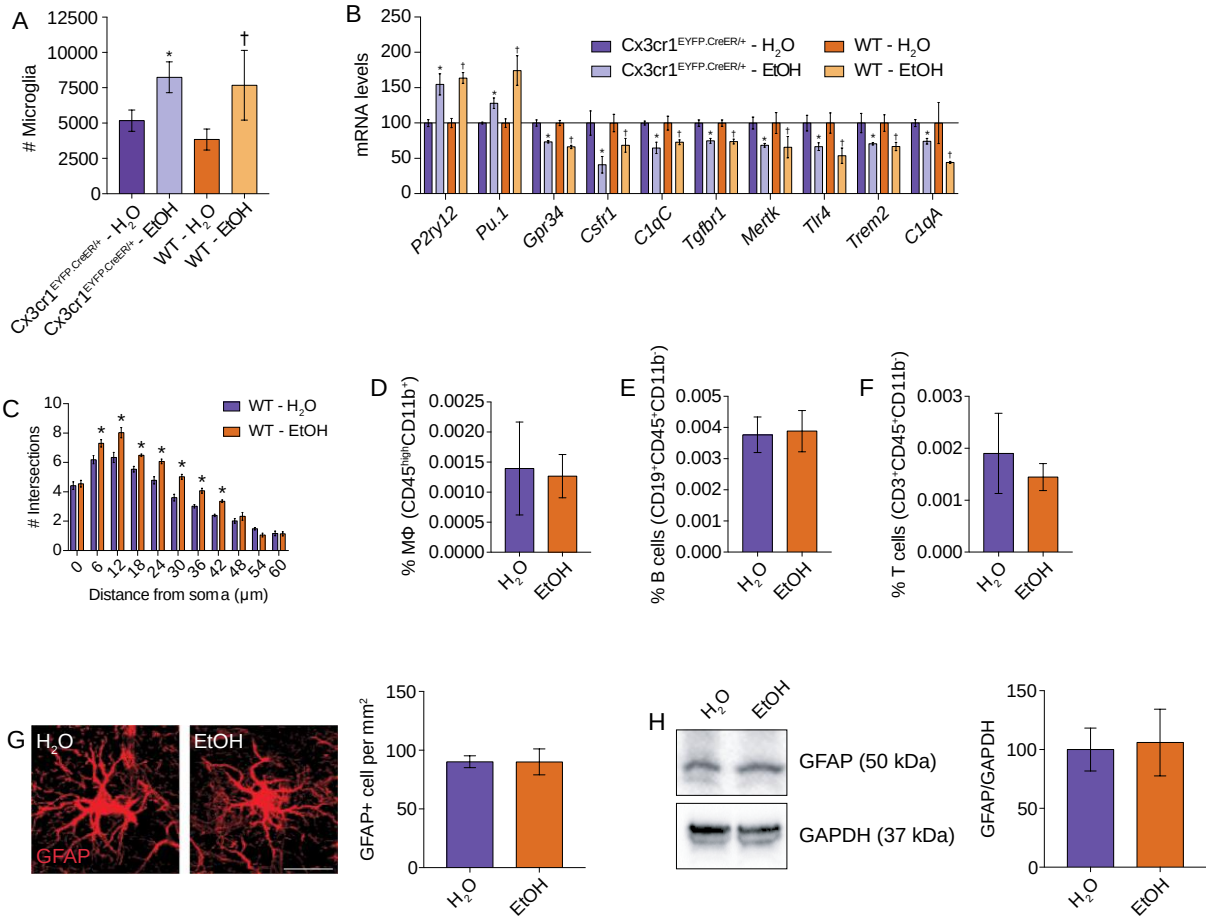

Fig. S1. Alcohol exposure does not activate other resident immune cells in the neocortex. (A) Flow cytometry analysis of microglial numbers in neocortices of Cx3cr1$^{EYFP\text{-}CreER/+}$ and WT mice exposed to EtOH or H_2O (n=5 mice per condition). Graphs (mean ± SEM) show microglia cell counts. Cell debris was excluded by size. *P<0.05 vs. Cx3cr1$^{EYFP\text{-}CreER/+}$ H_2O, and †P<0.05 vs. WT H_2O, by one-way ANOVA with Sidak´s correction. **B,** qRT-PCR from neocortices of Cx3cr1$^{EYFP\text{-}CreER/+}$ and WT mice exposed to EtOH or H_2O. Graph (mean ± SEM, n=5 mice per condition) shows the mRNA expression for the indicated transcripts. *P<0.05 vs. Cx3cr1$^{EYFP\text{-}CreER/+}$ H_2O, and †P<0.05 vs. WT H_2O, by one-way ANOVA with Sidak´s correction. **(C)** Sholl analysis retrieved from histological confocal images of Iba1 on tissue sections from prefrontal cortices of WT mice exposed to EtOH or H_2O. Data are mean ± SEM from 15 cells for each distance from 3 mice per condition pooled across 3 independent experiments. *P<0.05 by two-way ANOVA with Sidak´s multiple comparisons. **(D to F)** Flow cytometry analysis of macrophages and B and T lymphocytes in neocortices of Cx3cr1$^{EYFP\text{-}CreER/+}$ mice exposed to EtOH or H_2O (n=8 mice per condition). Graphs (mean and SEM) show cell counts. Cell debris was excluded by size. Data were statistically analyzed by Mann-Whitney test. **(G)** Confocal image of astrocyte on tissue sections from prefrontal cortices of Cx3cr1$^{EYFP\text{-}CreER/+}$ mice exposed to EtOH or H_2O (n= 5 mice per condition). Graph (mean ± SEM) shows the number of astrocytes (GFAP^{+} cells), statistically analyzed by Mann-Whitney test. Scale bar: 20 µm. **(H)** Western blot for GFAP on lysates from prefrontal cortices of Cx3cr1$^{EYFP\text{-}CreER/+}$ mice exposed to EtOH or H_2O (n=5 mice per condition). Graph (mean ± SEM) shows normalized ratio of GFAP to GAPDH (loading control), statistically analyzed by Mann-Whitney test. Data are related to Figure 1.

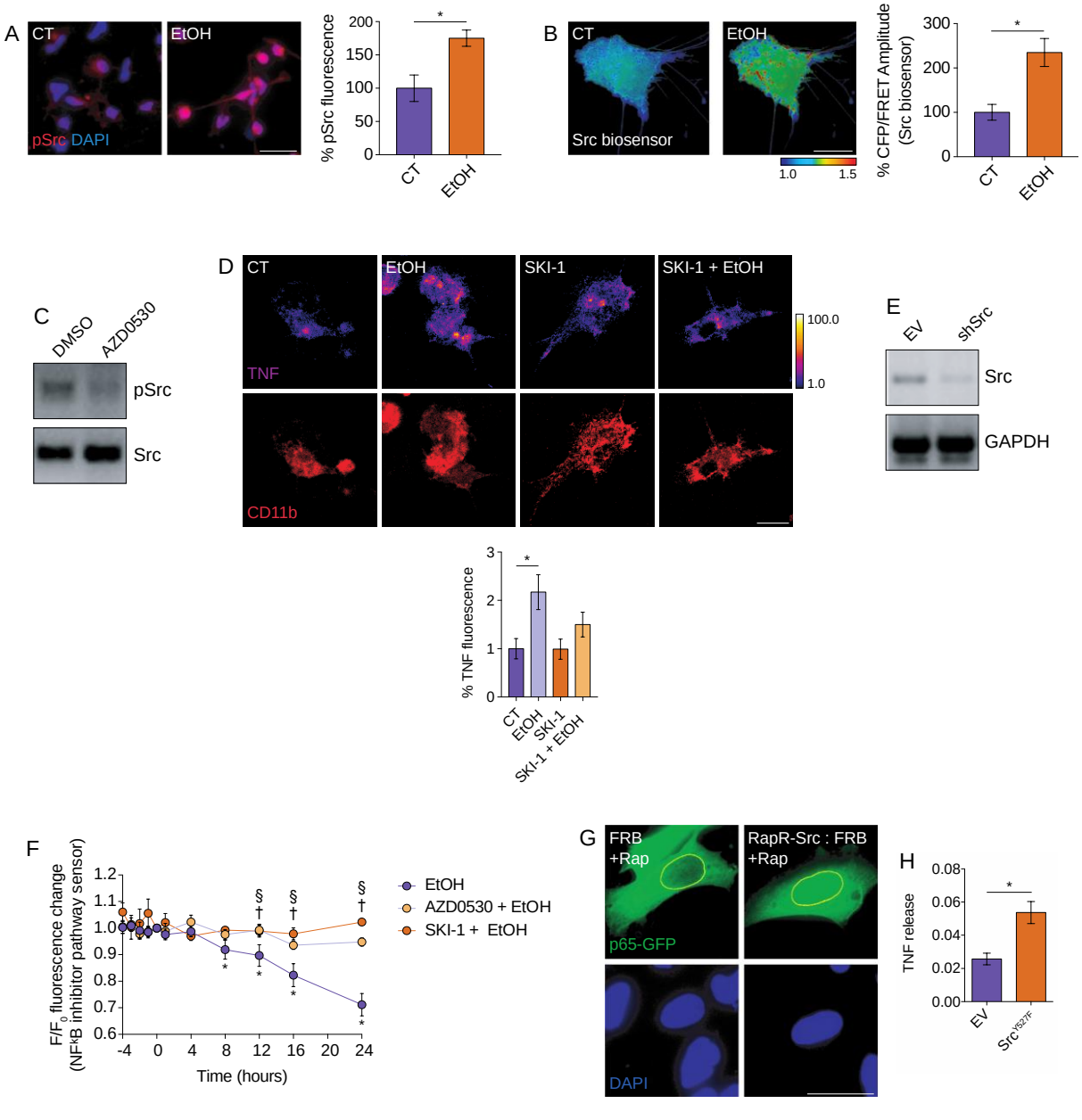

Fig. S2. Alcohol exposure modulates microglial TNF production through an Src–NF-κB pathway. (A) Primary cortical microglial cultures were treated with EtOH (70 mM) or H_2O (n=14 independent cultures) for 24 hours and immunostained for phospho-Src Tyr^{416} (red). Graph (mean ± SEM) displays the normalized pSrc fluorescence intensity per individual microglia in each cell culture. *P<0.05 by Mann-Whitney test. **(B)** CHME3 microglial cells expressing a Src FRET biosensor (KRas Src YPet) were recorded under basal condition (in the presence of HBSS) and then were challenged with 70 mM EtOH. Data are from n=25 cells pooled across 5 independent experiments. CFP/FRET emission ratios of the biosensor were normalized at 0 min. The panels show time-lapse CFP/FRET images coded according to the indicated pseudocolor scale. Graph displays the normalized maximum CFP/FRET amplitude in EtOH vs. HBSS. *P<0.05 by Mann-Whitney test. Scale bar: 10 µm. **(C)** Western blot for phospho-Src Tyr^{416} and Src on lysates from neocortices of Cx3cr1$^{EYFP\text{-}CreER/+}$ mice treated with DMSO or AZD0530. Gels are representative of 5 mice per condition. **(D)** Primary cortical microglial cultures were treated with EtOH (70 mM) or H_2O for 24 hours and immunostained for TNF. Graph (mean ± SEM, n=6 independent cultures) displays the normalized TNF fluorescence intensity per individual microglia in each cell culture coded according to the indicated pseudocolor scale. *P<0.05 ^{by} one-way ANOVA with FDR correction. Scale bar: 10

μm. **(E)** Western blot for phospho-Src Tyr^{416} and total Src on lysates from CHME3 microglial cells expressing a vector coding for Src shRNA or a control (pLKO) vector (gels are representative of 4 different cultures). **(F)** CHME3 microglial cells expressing a NFkB pathway inhibitor biosensor were recorded under basal condition (in the presence of HBSS) and then were challenged with 70 mM EtOH. Data are from n=15 cells per condition pooled across 3 independent experiments. Fluorescence signal of time lapses was normalized at 0 min in each experimental group. *P<0.05 vs. EtOH 0 min; §P<0.05 AZD + EtOH vs. EtOH at each related time point; and †P<0.05 SKI-1 + EtOH vs. EtOH at each related time point; by two-way ANOVA with Sidak´s multiple comparisons. **(G)** CHME3 microglial cells co-expressing a GFP-tagged p65 NFkB subunit (p65-GFP) with Src chemogenetic constructs (FRB + RapR-Src) or control constructs (FRB + FKBP) were treated with rapamycin (200 nM) and EtOH (70 mM) or H_2O for 24 hours. Graph displays the nuclear GFP fluorescence intensity per cell, from n=12 independent cultures. *P<0.05 by Mann-Whitney test. Scale bar: 20 μm. **(H)** ELISA on the culture media of N9 microglial cultures treated for 24 hours with EtOH (70 mM) or H_2O. Graph (means ± SEM, n=4 independent cultures) displays TNF content in ng/ml. *P<0.05 by Mann-Whitney test. Data are related to Figure 4.

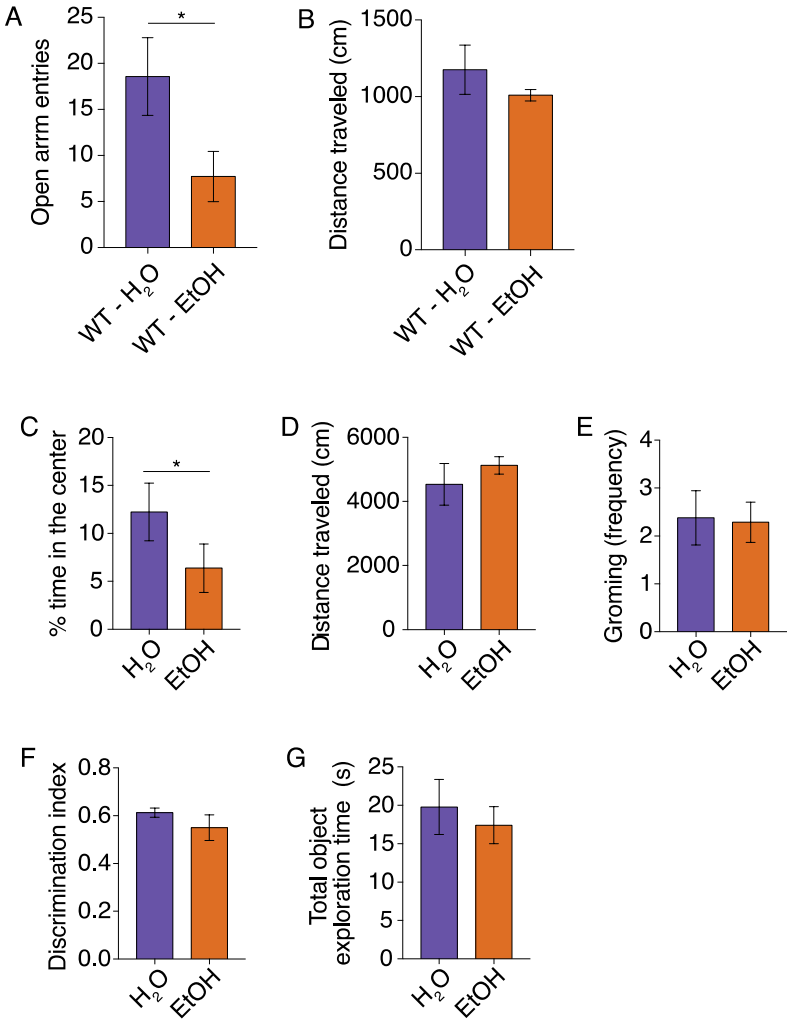

Fig. S3. Alcohol exposure does not alter general locomotor activity or recognition memory. (A and B) WT mice were exposed to EtOH or H_2O and then evaluated in the elevated-plus maze (EPM) test. Graphs (mean ± SEM, n=7 mice per condition) show the frequency of entries in the open arms (A) and total distance mice travelled in the maze (B). *P<0.05 by Mann-Whitney test. **(C to E)** $Cx3cr1^{CreER/+}$ mice were exposed to EtOH or H_2O and then evaluated in the open field arena. Graphs are mean ± SEM from n=8 mice per condition and were statistically analyzed by Mann-Whitney test. **(F and G)** $Cx3cr1^{CreER/+}$ mice were exposed to EtOH or H_2O and then evaluated in the novel object recognition (NOR) test. Recognition memory was similar between genotypes. Graphs are mean and SEM from n=8 mice per condition and statistically analyzed by Mann-Whitney test. Data are related to Figure 5.

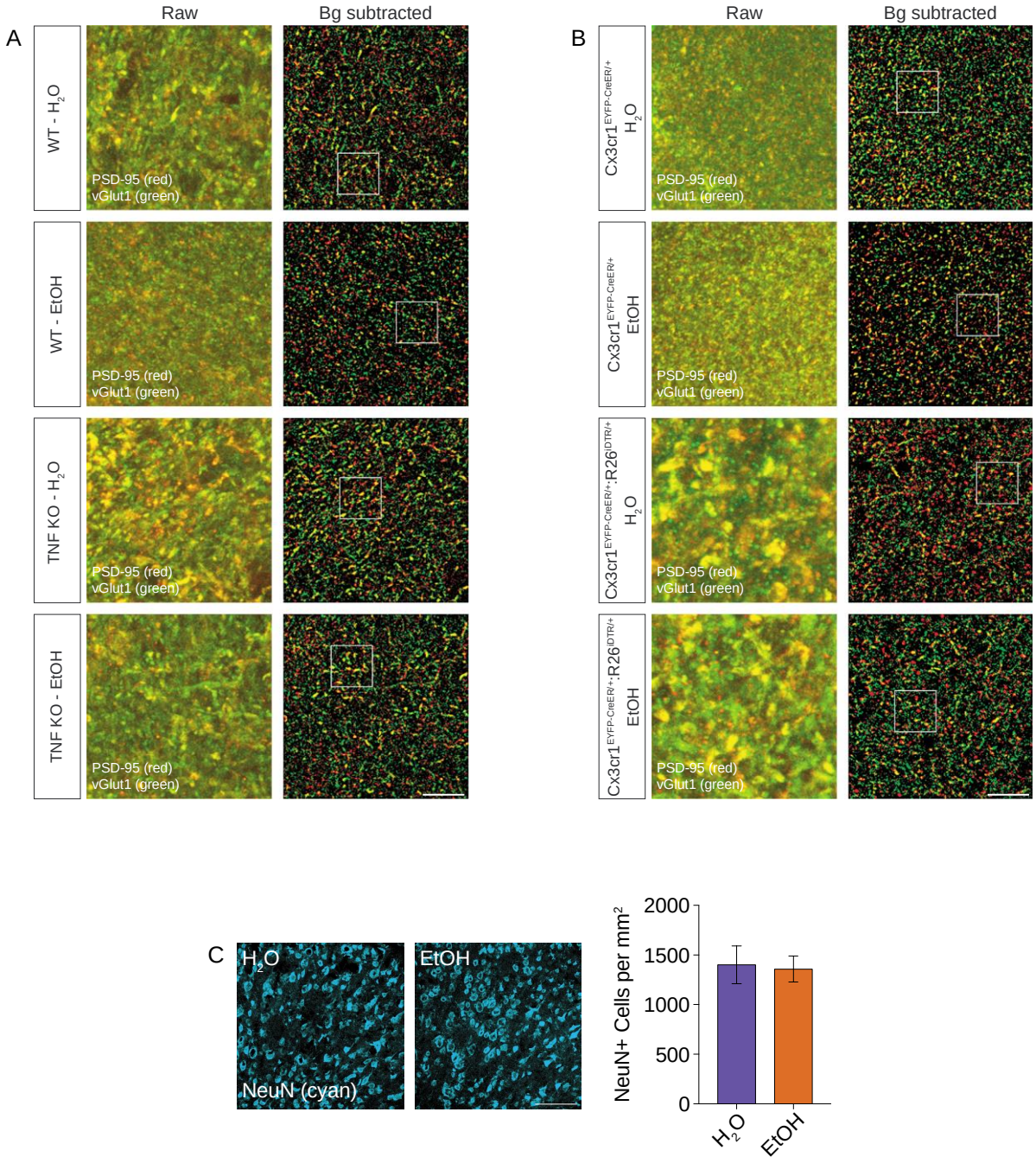

Fig. S4. Alcohol induces synapse loss without affecting neuronal numbers. (A and B) Representative raw and background-subtracted confocal images of PSD-95 (red) and vGlut1 (green) staining on tissue sections from prefrontal cortices of mice (genotypes noted in the boxes) exposed to EtOH or H_2O. White squares are the ROIs displayed on main Figure 6. Scale bar: 10 µm. **(C)** Histological confocal analysis of NeuN on tissue sections from prefrontal cortices of $Cx3cr1^{EYFP\text{-}CreER/+}$ mice exposed to EtOH or H_2O. Graph (mean and SEM, n=5 mice per condition) shows the number of NeuN+ cells. Data were statistically analyzed by Mann-Whitney test. Scale bar: 50 µm. Data are related to Figure 6.

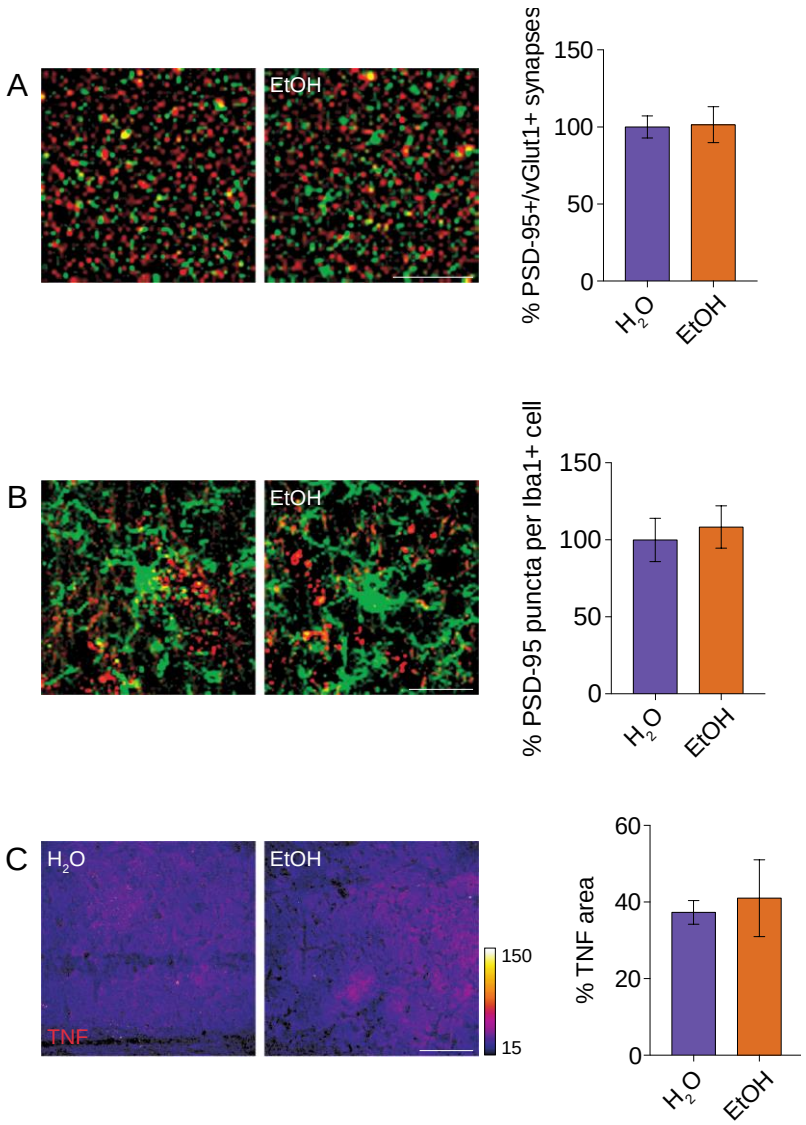

Fig. S5. Alcohol exposure does not alter synapse number, postsynaptic engulfment, or TNF production in the CA1 region of the dorsal hippocampus. (A) Histological confocal colocalization analysis for PSD-95 (red) and vGlut1 (green) on tissue sections from the CA1 region of the dorsal hippocampus of Cx3cr1$^{EYFP\text{-}CreER/+}$ mice after exposure to EtOH or H_2O. Graph (mean and SEM, n=6 mice per condition) shows the normalized number of excitatory synapses (yellow); data were statistically analyzed by Mann-Whitney test. Scale bar: 5 µm. **(B)** Histological confocal colocalization analysis for PSD-95 (red) and Iba1 (green) on tissue sections from the CA1 region of the dorsal hippocampus of Cx3cr1$^{EYFP\text{-}CreER/+}$ mice after exposure to EtOH or H_2O. Graph (mean and SEM, n=6 mice per condition) shows the normalized number of PSD-95 puncta engulfed by microglia (yellow); data were statistically analyzed by Mann-Whitney test. Scale bar: 10 µm. **(C)** histological confocal analysis for TNF on tissue sections from the CA1 region of the dorsal hippocampus of Cx3cr1$^{EYFP\text{-}CreER/+}$ after exposure to EtOH or H_2O. Graph (mean and SEM, n=5 mice per condition) shows the TNF protein expression coded according to the pseudocolor ramp. Data were statistically analyzed by Mann-Whitney test. Scale bar: 100 µm. Data are related to Figure 6.

Gene	FW	RV
P2ry12	CACCTCAGCCAATACCACCT	CAGGACGGTGTACAGCAATG
Pu.1	CAGTTCTCGTCCAAGCACAA	TTTCTTCACCTCGCCTGTCT
Csfr1	CCCTAGGACAAAGCAAGCAG	GATGTCCCTAGCCAGTCCAA
Tgfbr1	AAATTGCTCGACGCTGTTCT	TTCCTGTTGGCTGAGTTGTG
Mertk	GCCCACAATGACAAAGGACT	GGGAGTAGCCATCAAAACCA
Gpr34	GGTTGCTCTTGCTGGATTTC	CCGGGCTGTTGTAGCATATT
C1qA	GTGTGCTGACCATGACCCTA	ATTCCCCTGGGTCTCCTTTA
C1qB	AGACACAGTGGGGTGAGGTC	GGTCCCCTTTCTCTCCAAAC
C1qC	GAGGACCCAAGGGTCAGAAG	TGTATCGGCCCTCCACAC
Trem2	AACTTCAGATCCTCACTGGACC	CCTGGCTGGACTTAAGCTGT
Tlr4	GCTTTCACCTCTGCCTTCAC	GCGATACAATTCCACCTGCT
Tnf	GCCACCACGCTCTTCCTGTCT	TGAGGGTCTGGGCCATAGAAC
IL-6	CACAAGTCCGGAGAGGAGAC	CAGAATTGCCATTGCACAAC
Tlr2	TTGCTCCTGCGAACTCCTAT	GCTTTCTTGGGCTTCCTCTT
Tlr7	TGGAAATTTTGGACCTCAGC	TTGCAAAGAAAGCGATTGTG
CD14	GCTCAACTTTTCCTGCGAAC	CCCGCAGTGAATTGTGACTA
Mhc-II	ATGACCCAGGACCATGTGAT	ATCTTCCAGTTCACGCCATC
Ccl2	ATCCCAATGAGTAGGCTGGA	TCTGGACCCATTCCTTCTTG
Ccl5	GTGCCCACGTCAAGGAGTA	CCCACTTCTTCTCTGGGTTG
Icam1	CGAAGGTGGTTCTTCTGAGC	GTCTGCTGAGACCCCTCTTG
Tspo	TGGGAGGTTTCACAGAGGAC	GCCAGGTAAGGGTACAGCAA
Cox-2	GCTGTACAAGCAGTGGCAAA	CCCCAAAGATAGCATCTGGA
Irak3	TGGAGGTTCTAACGGGCTG	CCATCAGTTCCATGAGGAGGTC
Tnxnrd1	CAGGGTGACTGCTCAATCCACAAAC	CTCTTCCTACCGCCAGCAACACTG
Hmox1	GAAGGGTCAGGTGTCCAGAGAAGG	CGCTCTATCTCCTCTTCCAGGGC
Gclc	CACAGACCCAACCCAGAG	TGGCACATTGATGACAACCT
Slc23a2	CACTGATAGAAGTGGTCAT	AACACTAGGAAAATCGTCAG
Gr	CACGACCATGATTCCAGATG	CAGCATAGACGCCTTTGACA
Traf2	AGAGAGTAGTTCGGCCTTTCC	GTGCATCCATCATTGGGACAG
Rip1	GAAGACAGACCTAGACAGCGG	CCAGTAGCTTCACCACTCGAC
Nik	TGTGGGAAGTGGGAGATCCTA	GGCTGAACTCTTGGCTATTCTCA
Traf1	AGGGTGGTGGAATTACAGCAA	GCAGTGTAGAAAGCTGGAGAG
IL-1b	GCCCATCCTCTGTGACTCAT	AGGCCACAGGTATTTTGTCG
IL-18	CAGACAACTTTGGCCGACTT	GGGTTCACTGGCACTTTGAT
Inf-b	CAGCTCCAAGAAAGGACGAAC	GGCAGTGTAACTCTTCTGCAT
Cx3cl1	AAATGCGAAATCATGTGCGAC	CCTGGTTTAGCTGATAGCGGAT
Cxcl1	CTGGGATTCACCTCAAGAACATC	CAGGGTCAAGGCAAGCCTC
CD163	TGGTGTGCAGGGAATTACAA	AGCTCCACTCTTCCCTCACA
Arg1	CTCCAAGCCAAAGTCCTTAGAG	AGGAGCTGTCATTAGGGACATC
Nrlp3	ATGCTGCTTCGACATCTCCT	AACCAATGCGAGATCCTGAC
Socs3	CCCTTGCAGTTCTAAGTTCAACA	ACCTTTGACAAGCGGACTCTC

Mrp8	GCGCGGACAAATGACTCTG	CACTAGGCAAGCAAGTGAGGT
Mrp14	ATACTCTAGGAAGGAAGGACACC	TCCATGATGTCATTTATGAGGGC
Cxcl10	CCAAGTGCTGCCGTCATTTTC	GGCTCGCAGGGATGATTTCAA
Nos2	GTTCTCAGCCCAACAATACAAGA	GTGGACGGGTCGATGTCAC
Spp1	AGCAAGAAACTCTTCCAAGCAA	GTGAGATTCGTCAGATTCATCCG
Adam12	TGGGACCAGAGAGGAGCTTAC	GTTGCACAGTCAGCACGTCT
CD93	ATCTCAACTGGTTTGTTCCTGC	ACTCTTCACGGTGGCAAGATT
Ccr1	CTCATGCAGCATAGGAGGCTT	ACATGGCATCACCAAAAATCCA
Siglec1	CAGGGCATCCTCGACTGTC	GGAGCATCGTGAAGTTGGTTG
Axl	ATGGCCGACATTGCCAGTG	CGGTAGTAATCCCCGTTGTAGA
Mrc1	CTCTGTTCAGCTATTGGACGC	CGGAATTTCTGGGATTCAGCTTC
Apoe	CTGACAGGATGCCTAGCCG	CGCAGGTAATCCCAGAAGC
Cybb	TGTGGTTGGGGCTGAATGTC	CTGAGAAAGGAGAGCAGATTTCG
Lyz2	ATGGAATGGCTGGCTACTATGG	ACCAGTATCGGCTATTGATCTGA
Ywhaz	GATGAAGCCATTGCTGAACTTG	GTCTCCTTGGGTATCCGATGTC

Table S1. Primers. List of primers used in this study and their sequences (FW, forward; RV, reverse).